Summer 2012

Numerical investigation of plasma actuator configurations for flow separation control at multiple angles of attack

Thomas Kelsey West IV

Department:

NUMERICAL INVESTIGATION OF PLASMA ACTUATOR CONFIGURATIONS FOR FLOW SEPARATION CONTROL AT MULTIPLE ANGLES OF ATTACK

by

THOMAS KELSEY WEST IV

A THESIS

Presented to the Faculty of the Graduate School of the

MISSOURI UNIVERSITY OF SCIENCE AND TECHNOLOGY

In Partial Fulfillment of the Requirements for the Degree

MASTER OF SCIENCE IN AEROSPACE ENGINEERING

2012

Approved by

Dr. Serhat Hosder, Advisor
Dr. Joshua Rovey
Dr. Fathi Finaish

ABSTRACT

The primary objective of the study presented in this thesis was to analyze the effectiveness of aerodynamic plasma actuators as a means of active flow control over a low speed airfoil at multiple angles of attack each corresponding to two different flow separation mechanisms (i.e., laminar separation bubble and turbulent flow separation at stall conditions). Detailed parametric studies based on steady and unsteady Navier-Stokes simulations, modified to include the body force term created by the plasma actuator, were performed for a NACA 0012 airfoil at a chord Reynolds number of 10^5. In particular, parametric studies were performed to investigate the influence of the number, the location, the imposed body force magnitude (power input) and steady vs. unsteady operation of plasma actuators on the flow control effectiveness. First, the effectiveness of plasma actuators was studied when applied to the airfoil at a relatively low angle of attack, which involved the development of a laminar separation bubble (LSB). Next, the effectiveness of plasma actuators was analyzed at a high angle of attack where the stall of the airfoil occurs with a fully turbulent flow assumption. The results show that plasma actuators can provide significant improvement in aerodynamic performance for the flow conditions considered in this study. For LSB control, as much as a 50% improvement in the lift to drag ratio was observed. Results also show that the same improvement can be achieved using an unsteady or multiple actuators, which can require as much as 75% less power compared to a single, steady actuator. For the stalled airfoil case, as much as a 700% improvement in L/D was observed from a single, steady actuator. Note that this was achieved using a power input eight times higher than what was used for LSB control. Also, unsteady and multiple actuator configurations do not provide the same enhancement as the single, steady actuators. This was found to be due to the nature of the turbulent separation (trailing edge separation) at the stall condition that occurs for the selected airfoil and Reynolds number.

ACKNOWLEDGMENTS

I would like to sincerely thank my advisor, Dr. Serhat Hosder, for the opportunity and honor he has bestowed upon me by working with me on this research. He has given me the utmost dedication and guidance in developing me into not only a better student and researcher, but also a better person.

I would also like to thank my committee members, Dr. Joshua Rovey and Dr. Fathi Finaish for their dedication, support and time commitment to this research.

Furthermore, I would like to thank the Department of Mechanical and Aerospace Engineering at the Missouri University of Science and Technology for a great educational opportunity, as well as the provided facilities and funding. I would also like to thank the NASA-Missouri Space Grant Consortium for funding towards this research.

Finally, I absolutely must thank my family, friends and girlfriend for their love and support over the course of my education. Without them, I would not be where I am today, and this research would not have been possible.

TABLE OF CONTENTS

LIST OF ILLUSTRATIONS

Page

LIST OF TABLES

Page

NOMENCLATURE

Symbol	Description
C_p	Pressure Coefficient
St	Strouhal Number
f	Actuator Frequency (Hz)
c	Chord Length (m)
L_{sep}	Length of the Separation Region (m)
U_∞	Free-Stream Velocity (m/s)
T_f	Fundamental Actuation Period (seconds)
V	Actuator Input Voltage (kV)
L/D	Lift to Drag Ratio
ρ	Density (kg/m^3)
$\bar{V}$	Velocity (m/s)
P	Pressure (N/m^2)
μ	Dynamic Viscosity (kg/m-s)
$\bar{f}$	Body Force Vector (N/m^3)
ρ_c	Charge Density (C/m^3)
$\bar{E}$	Electric Field (N/C)
F_B	Actuator Body Force (mN/m)
LSB	Laminar Separation Bubble
UDF	User Defined Function

1. INTRODUCTION

The following chapter outlines the subsequent research on the computational modeling and application of aerodynamic plasma actuators. First, a description of the functionality and applications of plasma actuators are discussed. Next, a literature review regarding previous computational research in the area of plasma actuators was performed. Then, the objectives of the study are explained in great detail followed by a description of the contributions to the area of computational analysis of plasma actuators from this study. Lastly, an outline of the remainder of this thesis is provided.

1.1. AERODYNAMIC PLASMA ACTUATORS

In recent years, the area of active flow control techniques in aerodynamics has been a great topic of interest. Among these techniques is the aerodynamic plasma actuator. This device has been demonstrated to have great effectiveness in improving aerodynamic performance in flow scenarios involving flow separation and boundary layer control [1]. Examples of these scenarios include, but are not limited to, the flow separation that occurs at the stall angle of attack of an airfoil, separation around a cylinder, and the separation of the laminar boundary layer. The single dielectric barrier discharge (SDBD) plasma actuator [2], shown in Figure 1.1, is a relatively simple device consisting of a pair of electrodes separated by a dielectric material, typically arranged in the asymmetric configuration shown in Figure 1.1. In experiments conducted by Corke et al. ([3] and [4]) the electrodes were made of a copper foil tape, while the dielectric material was made of a kapton film. Other dielectric materials can be used such as Macor, Teflon or even glass. The differences between the materials are their breakdown voltages and ductility. The ductility affects the integration of the actuator, as those dielectrics with low ductility such as Macor cannot be easily integrated on curved surfaces [3]. In typical aerodynamic applications, one of the electrodes is exposed to the air, while the other is embedded in some surface, such as the skin on an aircraft wing, completely covered by the dielectric material.

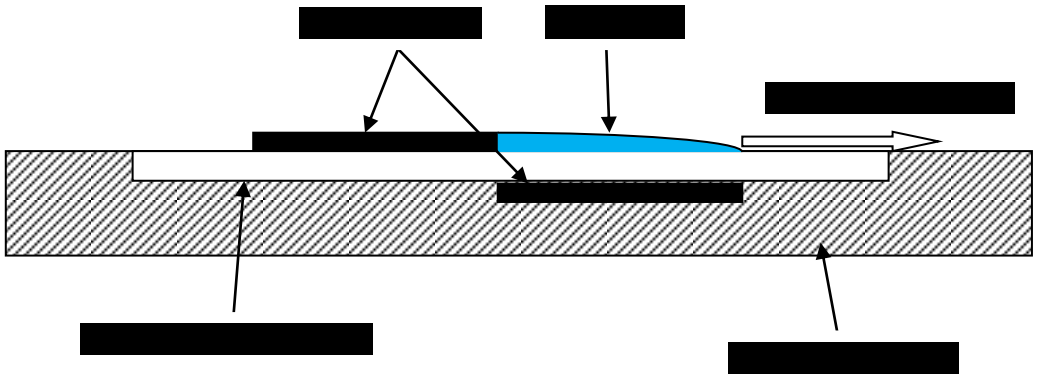

Figure 1.1: Single Dielectric Barrier Discharge Plasma Actuator

When an AC voltage is applied across the electrodes, and the frequency is large enough, the air ionizes in the region with the largest electric potential. As shown in Figure 1.1, this region is located above the embedded electrode, beginning near the edge of the exposed electrode. The ionized air, or plasma, in the presence of an electric field gradient, produces a body force on the ambient air [3], directed away from the exposed electrode, parallel to the dielectric material.

In order to ionize the air using the plasma actuator, it is required that a large, typically between 10 and 20 kV, AC voltage be applied across the electrodes, operating with an input frequency of 1-10 kHz [5]. Because of the large frequencies, plasma actuators can be regarded as "quasi-steady" devices, as these frequencies are typically well above the fluid response frequency [4]. Even with the large voltage demands, plasma actuators are relatively low power devices, operating around 2-40 Watts per foot of actuator span [3]. Enloe et al. [5] describe, in great detail, the electro-magnetic phenomenon governing plasma actuators.

Plasma actuators have many advantages over other flow control devices. First, plasma actuators can be used as an active flow control device. This means that they can be used in a time of need, and not in constant, uncontrolled use as with, for example, passive vortex generators [6]. One of the greatest advantages is that, when properly integrated, plasma actuators have almost no effect on the flow when in the off position as the exposed electrode is typically less than 0.1 mm thick. Also, from a mechanics stand

point, plasma actuators have no moving parts, making them solid-state devices, which are much simpler than mechanical devices with moving parts.

In contrast, there are disadvantages to plasma actuators. One substantial disadvantage is that because of the large voltage requirements necessary to drive plasma actuators, large, heavy amplifiers are typically required for adequate voltage supply. In the case of an unmanned aerial vehicle, a large amplifier may not be feasible, or the costs in weight and increased vehicle size outweigh the gain in aerodynamic performance. Further research may be required in the area of amplifier design and performance to eliminate this issue. Also, significant research is still required in the techniques of proper integration of plasma actuators into aerospace vehicles such that they cause minimal adverse flow disturbance. A large actuator profile above the surface of the airfoil may inadvertently trip the flow causing premature separation or an early transition to turbulent flow increasing the skin friction drag. Either or both of these adverse effects could require more power to control, or even make the plasma actuator ineffective.

1.2. LITERATURE REVIEW

1.2.1. Numerical Modeling of Plasma Actuators. Recently, an increasing amount of research has gone into the study of plasma actuators using numerical simulations. The biggest challenge with simulating plasma actuators remains to be modeling the actual behavior of the actuator, its effects on the surrounding flow field, and the distribution of the plasma region. Many different numerical models have been developed as the ongoing research in the area of plasma actuators expands. Suzen et al. [1] made use of a model based on Maxwell's equations stating the body force produced by the plasma actuator is a function of the charge density and the strength of the electric field produced by the actuator. In the same study, the plasma distribution over the embedded electrode was modeled using half of a Gaussian distribution, which was stated to represent previous experimental results. This model is considered to be a high fidelity model that represents the performance of the actuator based on the physics. On the other hand, Aholt and Finaish [8] incorporated a body force source term into the Navier-Stokes equations. Even though this model was not based on the actual physical representation of the physics governing the actuator (i.e., the solution of Maxwell Equations), this simple,

but useful, model was successfully used to demonstrate the effectiveness of using plasma actuators as a means of active flow control.

In terms of simulating the flow around plasma actuators, many different methods have, again, been implemented. Because flow separation is an unsteady phenomenon and related to turbulence transition, only Large-Eddy Simulations (LES) or Direct Numerical Simulations (DNS) can resolve the flow structure. Visbal et al. [9] has shown that the use of implicit LES simulations perform well when simulating the effects of plasma actuators on flow fields with large separation regions, such as the stall of an airfoil. However, LES and DNS methods are very computationally expensive. If it is not desired to clarify the turbulence structure, but rather to study the basic effects of plasma actuators, Reynolds-Averaged Navier-Stokes (RANS) simulations provide sufficient qualitative data [10].

RANS simulations have been performed in several studies using a variety of turbulence models. Corke et al. [2] performed an analysis of the effects of a plasma actuator on a NACA 0021 airfoil using the v^2-f turbulence model. In this study, a single, steady state actuator was placed very near the leading edge of the airfoil. The analysis was performed around the peak of the lift curve, at multiple angles of attack. These results show a shift in the lift curve. The actuator increases maximum lift coefficient about by about 15% and angle at the maximum lift coefficient increases approximately 4 degrees.

In another study by Aholt and Finaish [8], a parametric RANS simulation study was performed to determine the plausibility of using plasma actuators as a means of active flow control of laminar separation bubbles over an elliptical airfoil. In this study, the one equation Spallart-Allmaras turbulence model was implemented to simulate the turbulent flow at a chord Reynolds number of 10^5. Results of this study indicated as much as a 60% improvement in L/D when using a single, steady state actuator.

In another study by Tsubakino et al. [10], an analysis of a NACA 0012 airfoil was performed using the algebraic Baldwin and Lomax turbulence model. Here the effect of plasma actuators was studies at 16 degrees angle of attack, which was two degrees past the peak of the lift curve. The first part of the analysis was performed using a single, steady actuator placed at three locations along the upper surface of the airfoil at two force magnitude levels. Results show that, in general, the actuator placed closest to the leading

edge has the most influence and can best control the flow at each power level. An additional analysis was performed using two lower powered actuators. The results indicate that the two actuator configuration at a low power level gave relatively the same effect as a single actuator operating at the same additive power as the two actuators. This indicates that even though the improvement in aerodynamic performance is quite similar, it may be more efficient to use a multiple actuator configuration to control separation as the required input voltage for the actuators can be less than a single, high-powered actuator.

1.2.2. Applications of Plasma Actuators. Plasma Actuators have been shown to be effective in a variety of applications other than airfoil separation control. Huang et al. [11] demonstrated separation control over low pressure turbine blades used in gas turbine engines at low Reynolds numbers (50,000 to 100,000) typical for high altitude cruise. Using "PakB" turbine blades, an experimental analysis was performed comparing the performance of a steady actuator versus an unsteady actuator. The results indicated that the unsteady actuator was more effective than the steady actuator in forcing the flow to reattach, and also required less power.

Benard et al. [12] showed that plasma actuators could be used to improve free shear layer mixing at a nozzle exit. This experiment used a 22 degree diffuser with a pair of symmetrically placed DBD actuators placed on the lips of the diffuser. Time-averaged results show significant enhancement of the jet spreading, jet core length reduction, and an increase in turbulent kinetic energy throughout the flow field. Both steady and unsteady actuators were analyzed in this study. The unsteady actuator performs particularly well in that the turbulence kinetic energy is greatly increased in the overall flow field due to the pulsing of the actuator.

Plasma actuators have also been used as devices for noise reduction. In a study performed by Thomas et al. [13], plasma actuators were used to study the plausibility of control flow separation over bluff bodies, in particular cylinders which are commonly found on aircraft landing gear. The results showed that the plasma actuators could be used to create an effective "plasma fairing." This resulted in an impressive reduction of separation and associated unsteady vortex shedding. In relation to the landing gear,

reducing flow separation could reduce the noise generated in the structure due to the separation.

1.3. OBJECTIVES OF THE CURRENT STUDY

In this study, flow separation control using plasma actuators over a NACA 0012 airfoil at a chord Reynolds number of 100,000 is investigated. Using Computational Fluid Dynamics, the global objective was to study and evaluate the effectiveness of separation control using plasma actuators at multiple angles of attack with flow regimes corresponding to two different flow separation mechanisms (i.e., laminar separation bubble and turbulent flow separation at stall conditions). At the same Reynolds number, an examination of laminar separation bubbles at relatively low angles of attack (less than that of the stall angle), as well as fully turbulent, separated flows at the stall angle was necessary to fully characterize a range of performance and capabilities of aerodynamic plasma actuators. Controlling both types of separation was explored using a single actuator and multiple actuator configurations, changing the location of the actuators, and observing the effects of operating the actuators in a steady state mode versus an unsteady, or pulsed, mode of operation. It is important to note that the flow separations depicted and analyzed in this study are dependent on Reynolds number which influences the structure of the near-wall flow field and the separation. A change in the Reynolds number may affect the separation location, size of the separation region, and even the angles of attack that both the laminar and stall separations occur. The Reynolds number used in this study was chosen because this Reynolds number is typical for both manned and unmanned, high altitude flight vehicles and significant separation around the selected airfoil has been demonstrated [10].

Another objective of this study is to approximate the required plasma actuator inputs, voltage and frequency, necessary to control different flow separation mechanisms. While models have previously been developed [2] to represent the physics and approximate the body force produced by the plasma actuator, these models tend to be computationally expensive and are only models. In this study, an experimental correlation developed by Porter et al. [14] where the force per unit span generated by a plasma actuator is given in relation to voltage and frequency inputs. The outcome of this

objective should provide a basis for determining the necessary voltage and frequency inputs used in plasma actuator system design and experimental analysis.

1.3.1. Investigation of Laminar Separation Bubble (LSB) Control with Plasma Actuators. At angles of attack less than that of the stall angle, it is possible for flow separation to occur, particularly at the low Reynolds number investigated in this study. Shen et al. [15] performed direct numerical simulations around a NACA 0012 airfoil at a chord Reynolds number of 100,000 illustrating the presence of flow separation due to the detachment of the laminar boundary layer from the airfoil surface. This is caused by the presence of an adverse pressure gradient. The separated shear layer, in some cases, may undergo a rapid transition to turbulent flow which could cause the shear layer to reattach to the surface, forming an attached turbulent boundary layer. This yields the development of a laminar separation bubble. It is important to note that the formation of this bubble may not occur at all angles of attack. If the angle of attack is too low, the pressure gradient will not be large enough to induce laminar separation. On the contrary, if the angle of attack is too high the pressure gradient may be large enough such that laminar separation will occur, but without reattachment. The formation of this bubble, shown in Figure 1.2, can have an extremely detrimental effect on aerodynamic performance in that the separation bubble causes an increase in the pressure drag on the airfoil [8].

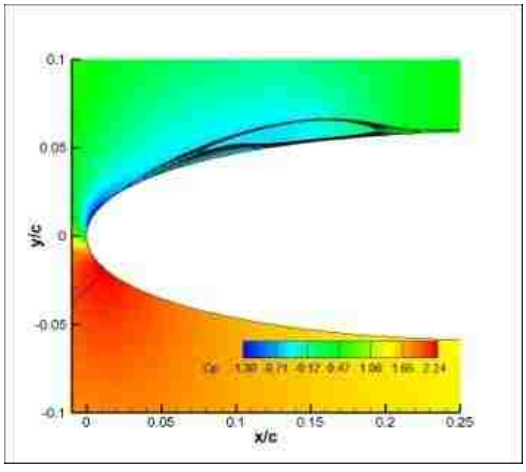

Figure 1.2: Leading Edge Laminar Separation Bubble at 8 Degrees Angle of Attack (Pressure Coefficient Contour with Streamlines)

1.3.2. Investigation of Turbulent Separation and Stall Control with Plasma Actuators. At the stall angle of attack, large scale separation occurs over nearly the entire upper surface of the selected NACA 0012 airfoil. This region of separation dramatically influences the lift and drag characteristics of the airfoil in a negative manner. For the given Reynolds number, it is assumed that the flow is fully turbulent at the stall angle, which was determined to be 15 degrees. This means that there is no longer an imposed laminar to turbulent transition region as with the previously discussed scenario. Physically, this represents a case in which the flow immediately transitions to turbulent flow upon reaching the airfoil, due to the large separation region. Figure 1.3 shows how the separation region forms with increasing angle of attack, as well as the magnitude of the developing separation region on the airfoil. Prior to 15 degrees, only a region of trailing edge separation occurs after formation of the previously discussed laminar separation bubble is no longer possible. The trailing edge separation begins to develop at about 10 degrees angle of attack and increases through 15 degrees where the separation region grows past the maximum thickness location (30% chord for this airfoil) and engulfs the entire upper surface of the airfoil. The objective of this portion of the study is to use aerodynamic plasma actuators to force the separation downstream such that separation region no longer covers the entire upper surface. With the use of leading edge actuators, it will likely not be possible to fully eliminate separation over the entire airfoil without an unrealistic power input. It is known that as the flow accelerates past the leading edge of the airfoil without separating, the flow will eventually reach an adverse pressure gradient near the point of the maximum velocity, causing a region of separation near the trailing edge [10]. Unless the flow is accelerated fast enough by the plasma actuator, flow separation will likely still occur downstream near the trailing edge. However, a separation region near the trailing edge has only a small influence on the aerodynamic characteristics of the airfoil.

The goal is to demonstrate that plasma actuators could be used as an active means of stall control when the flow field and separation region are fully turbulent. Adequate control of this type of flow could allow airfoils to reach higher angles of attack without large scale separation, which greatly improves the capabilities of the airfoil in terms of aerodynamic performance.

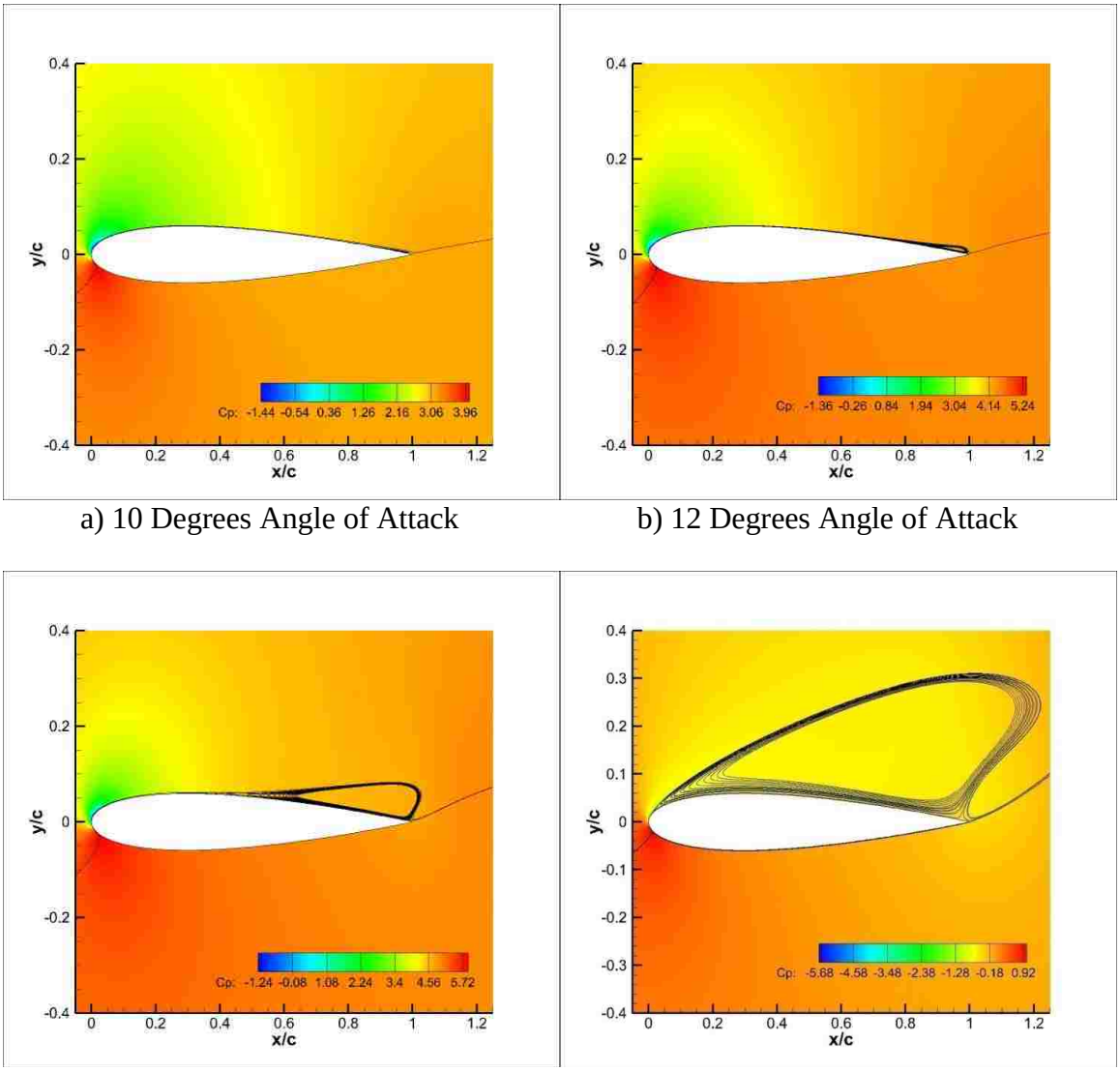

a) 10 Degrees Angle of Attack

b) 12 Degrees Angle of Attack

c) 14 Degrees Angle of Attack

d) 15 Degrees Angle of Attack

Figure 1.3: Stall Separation Bubble Development from 10 to 15 Degrees Angle of Attack (Pressure Coefficient Contour with Streamlines)

1.3.3. Investigation of the Effect of Plasma Actuator Location and Multiple Actuator Configurations on Flow Control Effectiveness. In some cases, the use of a single plasma actuator as a means of flow separation control may not be possible. In particular, flow separation at the stall angle of attack is strong and, after a perturbation, the fluid recovery time is extremely small. Here, the use of one actuator may delay the separation of the boundary layer, but if this delay is not sufficient, substantial flow

separation may still ensue. The application of multiple actuators could be used to further delay the separation point of the boundary layer by providing a longer distance over which momentum is added to the flow. With this, it may also be possible to reduce the power consumed by each actuator in an array compared to a single, higher powered actuator. One of the objectives of the current study is to investigate the plausibility of using an array of lower powered plasma actuators to control the two flow separation cases of interest in the study.

1.3.4. Investigation of the Effect of Steady vs. Unsteady Actuator Operation on Flow Control Effectiveness. As mentioned previously, plasma actuators can be regarded as a "quasi-steady" device. This implies that if the actuator was operated continuously, the fluctuations due to the AC voltage powering the device are negligible. It has been shown that the use of a "pulsed" actuator can provide significantly greater aerodynamic performance enhancement, even beyond that of a steady state actuator for certain cases [9]. The pulsing effect of the unsteady actuator can generate large coherent vortices that could delay or even prevent separation. These structures intermittently bring high momentum fluid to the surface, helping the flow withstand the adverse pressure gradient without separation [4]. One tremendous advantage to using a pulsed actuator is that the power requirement could be less than that of a steady actuator, and the gain in aerodynamic performance could be the same, if not better than a steady actuator [3], [4]. The objective is to make a comparison between steady and unsteady actuator operation for both the laminar and turbulent separation cases discussed above, as well as the multiple actuator configurations. In the cases of the multiple actuator configurations, the actuators were operated such that the actuators were offset by one actuation period. For example, if actuator 1 is on from t=1.0 seconds to t=1.1 seconds, then actuator 2 was operated from t=1.1 seconds to t=1.2 seconds, and so on. This would allow for the greatest time period in which momentum is being added to the flow by an actuator. Because of the success of using unsteady actuators to reduce the power consumed by single plasma actuators, an investigation of using lower powered unsteady, multiple actuators is performed compared to multiple, steady actuators.

1.4. CONTRIBUTIONS OF THE CURRENT STUDY

This study makes three main contributions to the field of using plasma actuators as a means of active flow control around airfoils. First and foremost is the demonstration of the use of plasma actuators across a range of angles of attack. Very little computational research has been performed across a range of angles of attack using plasma actuators. This is likely due to the fact the one single actuator, at one location may not have the capability to control the entire flow field from downstream laminar separation regions to the leading edge (or trailing edge) turbulent separation of a stalled airfoil as the separation location may be in a different location at each angle of attack. In light of this, the second major contribution will be demonstrating the effectiveness of multiple plasma actuators. A multiple actuator configuration could provide a means of active flow control in a dynamic environment, at least in the instance when realistic power needs are required.

The last contribution will be relating the inputs of a numerical simulation to the inputs of an actual plasma actuator. In many previous numerical analyses, inputs into numerical schemes have been electric field magnitudes and charge densities for complex models or simply momentum source term or body force magnitudes for simple models, each given with no relation to a physical application. While a more simplified approach to modeling the actuator will be used in this study, the results will be given in terms of actuator voltage and frequency, as these are the main input parameters for plasma actuator operation.

1.5. THESIS OUTLINE

The following document is divided four chapters. Section 2 focuses on computational method used to simulate the behavior and effect of plasma actuators. This includes an explanation of the numerical flow solver, solution methodology, boundary conditions and turbulence modeling. Furthermore, detail is given regarding the generation of the computational grid and determining the validity of the grid through a spatial or grid convergence study.

Sections 3 and 4 outline the results of the wide variety of the actuator configurations analyzed in the study. Section 3 deals with the control of low angle of

attack laminar separated flows, in particular, the scenario involving the formation of a laminar separation bubble. Section 4 gives the results for the control of fully turbulent flow at stall conditions. Each of the laminar and turbulent separation chapters are broken down into subsections to make comparisons between steady and unsteady actuators as well as a comparison between the use of a single actuator and multiple actuator configurations. Both comparisons will not only show the difference in aerodynamic performance, but also the required power input to achieve the control demonstrated for each actuator configuration.

In the last section, a conclusion is given to summarize the control of the flow around the selected airfoil across a range of angles of attack. Because this research can be expanded to a various range of actuator configurations, flow scenarios, flight conditions, etc. a suggested outline of future work is given.

The procedure used for setting up and running the numerical simulations used in this study is given in the appendix.

2. COMPUTATIONAL FLUID DYNAMICS MODEL

This section outlines the numerical methodology used to achieve the goals outlined for this study. First, a description of the computational method, flow solver and the developed computational grid are given along with the results of a conducted grid convergence study. Lastly, details are given with regards to boundary conditions, turbulence modeling and computational modeling of the plasma actuator.

2.1. SOLUTION METHODOLOGY AND FLOW SOLVER

The computational fluid dynamics (CFD) code used in this study for the numerical solution of steady and unsteady RANS equations is the commercially available solver ANSYS FLUENT 12 [16]. Eq. (1) and (2) are the conservation equations for mass and momentum, respectively that are solved numerically by the flow solver.

$$\frac{D\rho}{Dt} + \rho(\nabla \cdot \bar{V}) = 0 \tag{1}$$

$$\rho \frac{D\bar{V}}{Dt} = -\nabla P + \mu \nabla^2 \bar{V} \tag{2}$$

Here, $\bar{V}$ is the velocity field, ρ is the fluid density, P is the pressure and μ is the dynamic viscosity. Note here that $\frac{D}{Dt}$ is the material or total derivative. The selection of FLUENT was made due to the various solution capabilities, including the ease of incorporating a model to represent the plasma actuators through the use of a user defined function (UDF). UDFs allow for additions and/or alterations to the flow solver and governing equations by compiling subroutines and linking them to FLUENT. The solutions for this study were obtained using the pressure based, segregated solver. Second order spatial discretization was applied for pressure and momentum, as well as the selected turbulence model. The absolute convergence requirement of all residuals was set to 10^{-6}. For pressure-velocity coupling, the SIMPLE method was implemented. To handle the transient flow discretization, a second-order implicit time marching scheme was implemented for time integration of the solution. The details on the set-up of Fluent CFD model are given in the Appendix.

The convergence of each case was achieved by ensuring that each of the governing equations (mass and momentum) and the turbulence model equation converged to the prescribed absolute convergence requirement. For steady state cases, iterations were performed until the convergence requirement was met. For transient cases, convergence was achieved for each time step where the time step size was 0.01 seconds. Lift and drag data was then extracted from the converged cases. This is direct for steady flow cases as the lift and drag are a singular value. However, for unsteady cases periodic behavior of the lift and drag coefficients are observed. In order to determine the lift and drag for these cases, a mean of each is taken when the periodic motion is approximately centered about a single value with constant amplitude (i.e. after the flow has fully developed.)

2.2. GEOMETRY AND COMPUTATIONAL GRID

A symmetric NACA 0012 airfoil with a 1 meter chord length was the geometry of interest for this study. The geometry and computational grid were both constructed using a hyperbolic C-type grid generator [17] developed for constructing grids around airfoils. The grid size was 20 chord lengths from the origin, located at the leading edge of the airfoil, in every direction while the wall spacing to the first grid point from the airfoil surface was 2.3×10^{-5} m. This corresponds to a y+ value much less than one for the selected Reynolds number. The objective is to completely resolve the boundary layer, including the viscous sub-layer, without the use of wall functions as these are only approximations of the behavior of the near-wall region. The dimensions of the grid used in this study were 999x200 grid points, where the first number corresponds to the number grid lines in the streamwise direction and the second is the number of gridlines in the direction normal to the wall. The grid generator used a hyperbolic point distribution method parallel to the airfoil surface. The normal grid lines are, however, distributed evenly along the upper and lower surfaces. Figure 2.1 depicts various aspects of the computational grid. Figure 2.1a shows the full computational grid, Figure 2.1b shows the grid around the airfoil and Figure 2.1c shows the grid near the leading edge.

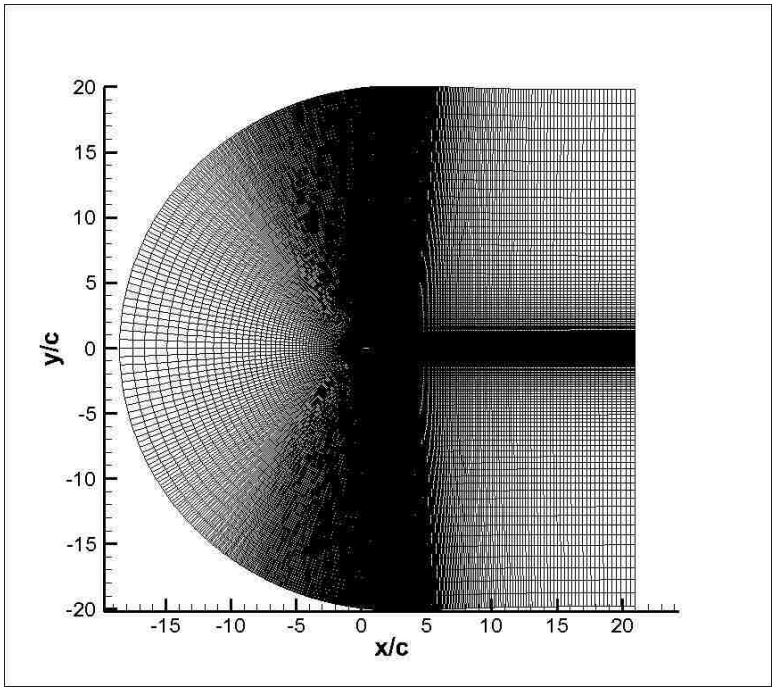

a) Full Grid View

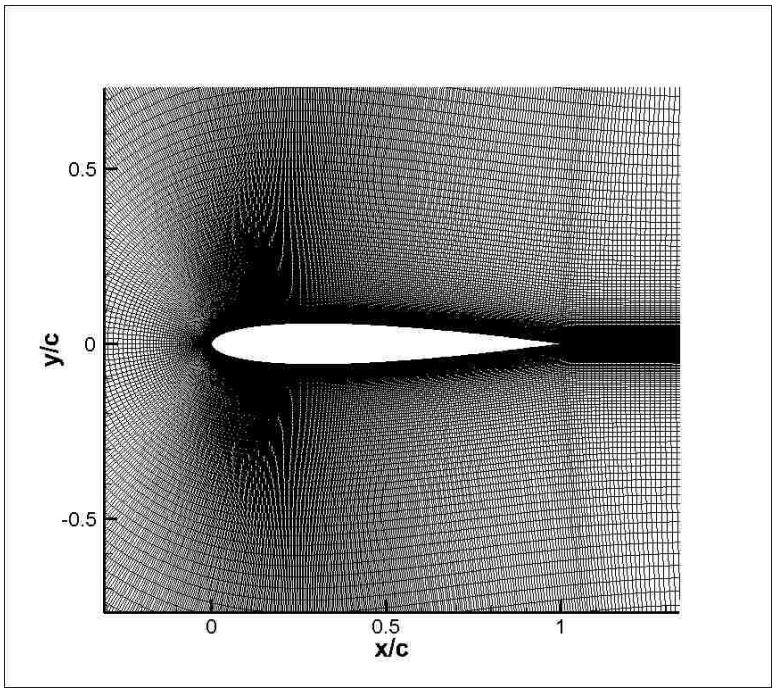

b) Airfoil View

Figure 2.1: Computational Grid

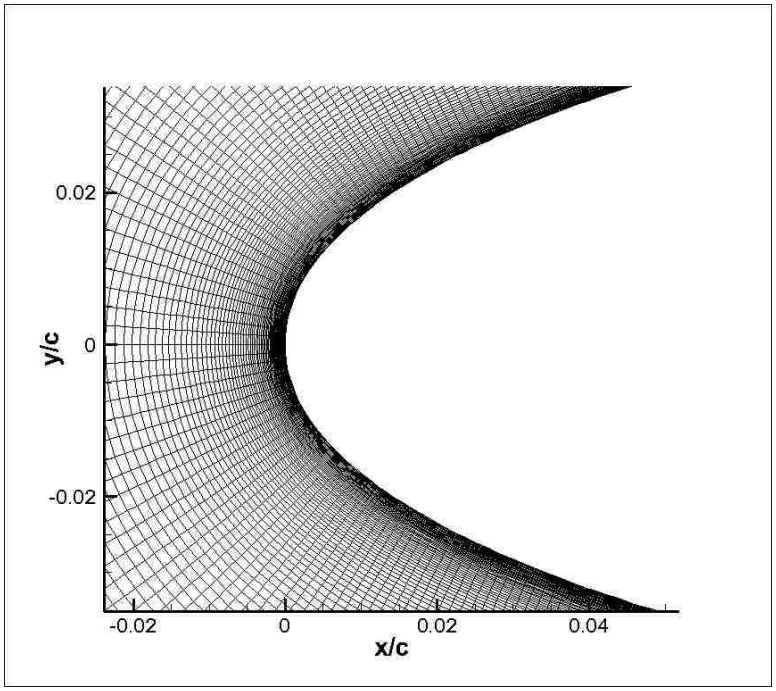

c) Near-Wall View of the LE Region

Figure 2.1: Computational Grid (cont.)

In order to confirm the spatial convergence the grid developed for this study, a grid convergence study was performed using two additional coarsened grids. Each grid's dimensions were determined by reducing the size by a factor of two at each level. While the main grid had dimensions 999x200, the next grid level had dimensions 499x100, and the coarsest grid had dimensions 249x50. To check the convergence of the computational grid, steady-state simulations were performed on each grid at angles of attack from 0 to 16 degrees. The lift and drag distributions for the grids, as well as the drag polar are shown in Figures 2.2. From these results, it can be seen that the convergence is achieved with the grid level to be used in this study. Only small deviations at the stall angles of attack occur, but this is to be expected. The use of a coarse grid in flows with large separation and circulation may have large residual error in the solution.

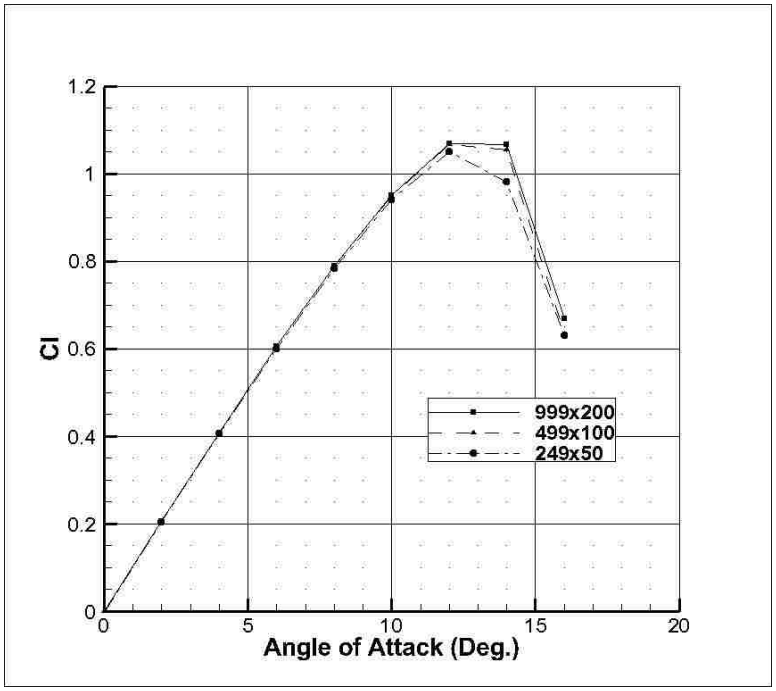

a) Cl vs. Angle of Attack

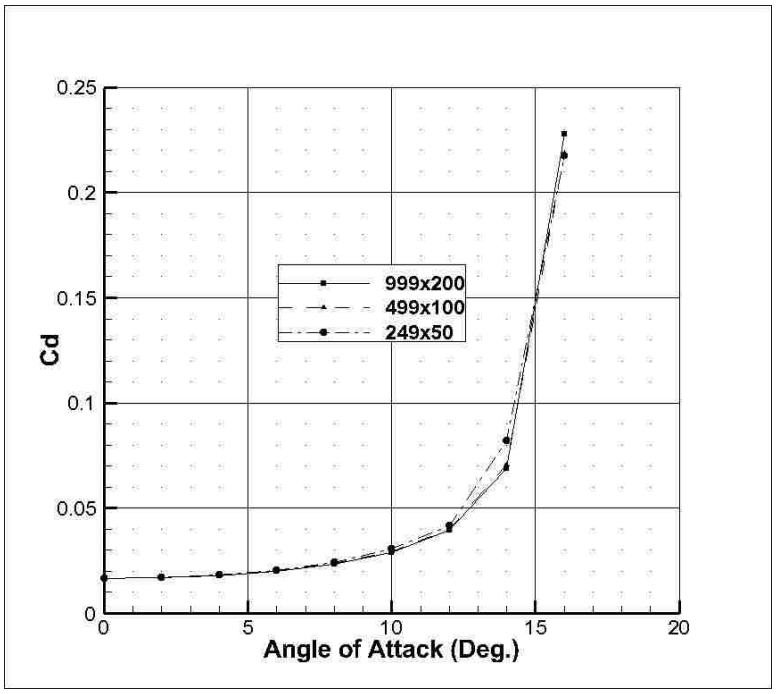

b) Cd vs. Angle of Attack

Figure 2.2: Gird Convergence Study Results for Cl vs. Angle of Attack, Cd vs. Angle of Attack and Cl vs. Cd

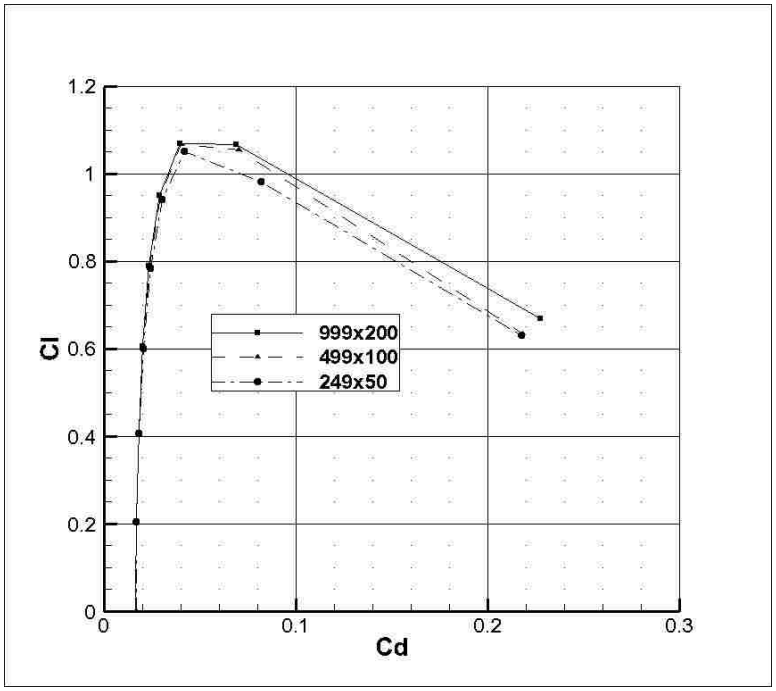

c) Cl vs. Cd

Figure 2.2: Gird Convergence Study Results for Cl vs. Angle of Attack, Cd vs. Angle of Attack and Cl vs. Cd (cont.)

In addition to the lift and drag characteristics, the pressure distributions and skin friction distributions along the airfoil were also compared for the three grid levels. The pressure and skin friction distributions were taken at three angles of attack, namely 2, 8 and 16 degrees. Pressure coefficient distributions are shown in Figures 2.3 for the three angles of attack, while Figures 2.4 show the skin friction coefficient distributions, again at the three angles of attacks. These results, again, show the grid convergence has been achieved for the finest grid. The pressure coefficient distribution plots match nearly exactly. There is some deviation in the skin friction coefficient distribution plots, but this difference minute. Confirming the grid convergence is achieved suggests that the residual error in the grid should be small which reaffirms the accuracy of the results forthcoming in this study and indicates that the solutions are independent of the computational grid.

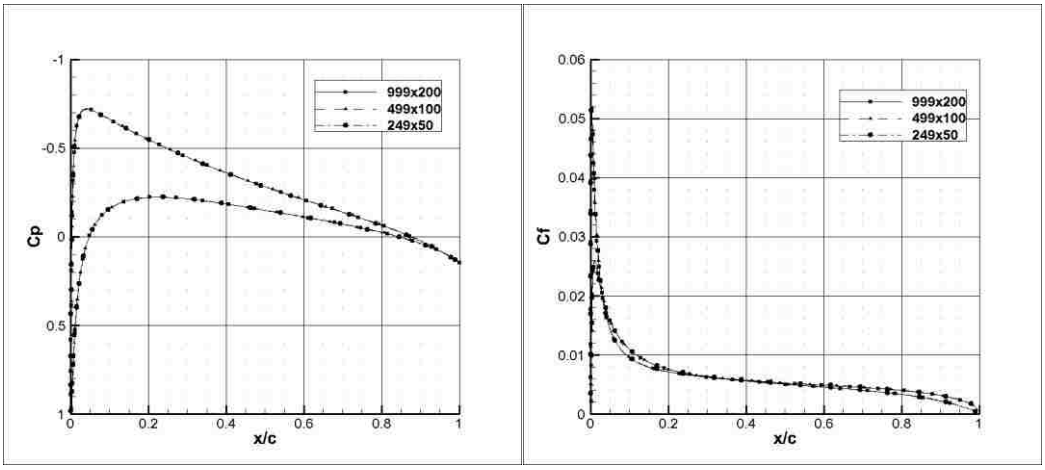

a) 2 deg. Angle of Attack

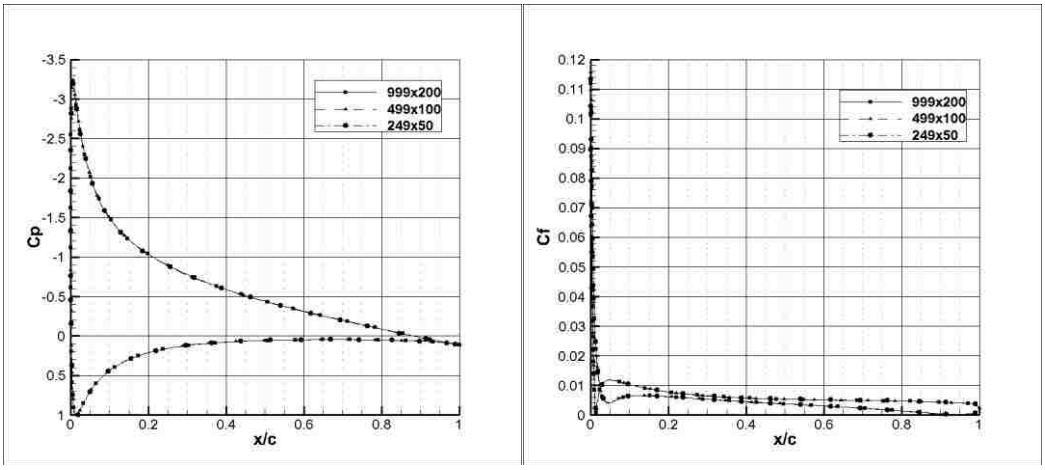

b) 8 deg. Angle of Attack

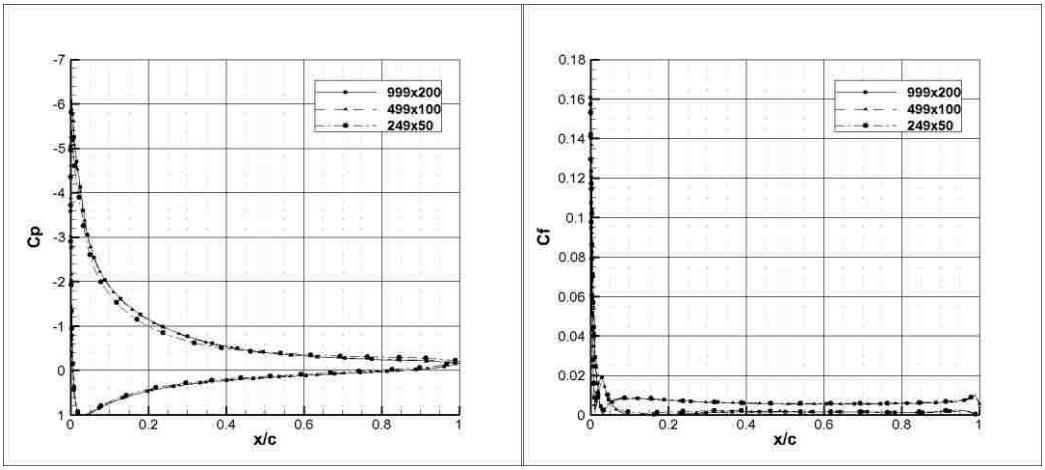

c) 14 deg. Angle of Attack

Figure 2.3: Grid Convergence Study Results for the Pressure Coefficient (Left) and Skin Friction Coefficient (Right) Distributions

2.3. BOUNDARY CONDITIONS

There are three main boundaries for the computational grid, shown in Figure 2.4. Two of these are the farfield boundary. The left-hand side, top and bottom edges were modeled as velocity inlets while the right edge of the grid was set as an outflow boundary. These boundary conditions are suitable for the low speed, incompressible flow analyzed in this study. The other boundary is the airfoil surface, which was modeled as a no-slip wall boundary. The inlet conditions were set such that free stream flow had a chord Reynolds number 100,000. Sea level density (1.225 kg/m^3) and dynamic viscosity (1.7894x10^{-5} kg/m-s) were used as the free-stream air properties. This corresponds to a free-stream velocity of 1.46 m/s.

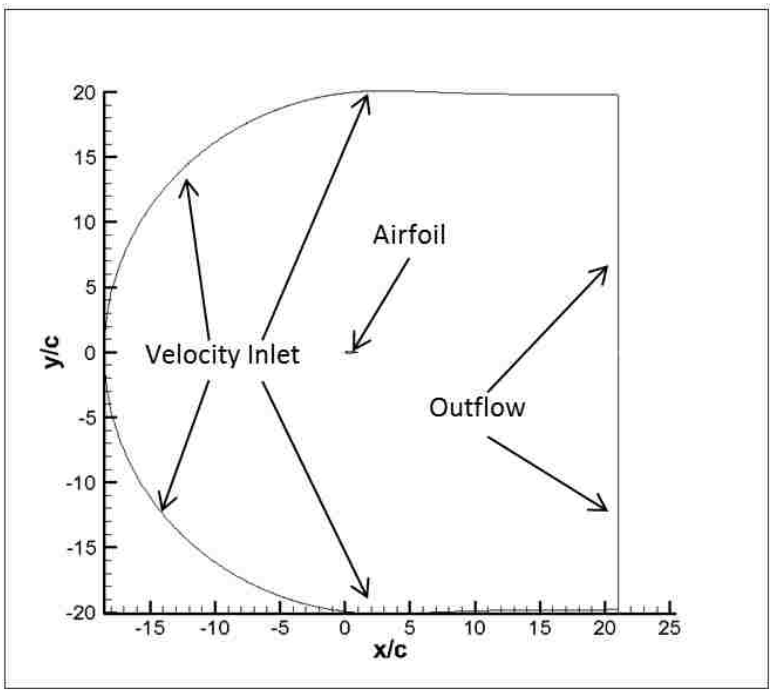

Figure 2.4: Computational Grid Boundaries

2.4. MODELING OF TURBULENCE AND TURBULENT FLOW TRANSITION

FLUENT 12 has a wide variety of models readily available, with an array of settings and correction factors. For this study, the one equation Spalart-Allmaras, Eddy-Viscosity model was employed to simulate the turbulent flow. Spalart and Allmaras [18]

have shown that this model performs well in flows with adverse pressure gradients and exhibits numerical robustness in complex flow simulations. Also, since this is a one equation model, it is computationally less expensive compared some other models, such as the four equation Transition SST model or the five equation Reynolds Stress model, both of which are available in FLUENT 12.

Because of the use of the Reynolds Averaged Navier-Stokes (RANS) equations by the FLUENT solver, special arrangements had to be made in order to model the laminar separation bubble formed at low angles of attack. Simple RANS modeling lacks the ability to accurately predict laminar to turbulent transitions. It is typical that when using RANS modeling, the transition location is specified by the user. In FLUENT, this was done by partitioning the computational grid into to two zones. The location of the partition varies depending on the location of the laminar separation, which is analogous to the angle of attack to the airfoil. The partition is placed at the location that causes the greatest aerodynamic performance loss while still forming the separation bubble for each selected angle of attack.

Although the transition location is imposed and does not naturally occur, this method is consistent with the physics associated with the laminar separation bubble formation phenomenon. This is also the procedure used by Aholt and Finaish [8] as part of their study of the control of laminar separation bubbles. In order to relax this assumption, higher fidelity computation methods such as Large-Eddy Simulations (LES), Detached-Eddy Simulations (DES), Direct Numerical Simulations or more complex RANS models would be necessary. However these methods are several times more computationally expensive than simple RANS modeling, especially when using a one-equation turbulence model.

2.5. PLASMA ACTUATOR MODEL

It is well understood that plasma actuators impart a body force on the flow. This is synonymous to simply adding momentum to the flow in a prescribed region. This region is approximately where the plasma is created by the actuator. To model a plasma actuator in FLUENT, a user-defined function (UDF) can be compiled into the solver,

adding a momentum source term to the governing equation for momentum [8] shown in Eq. (3).

$$\rho \frac{D\bar{V}}{Dt} = -\nabla P + \mu \nabla^2 \bar{V} + \rho \bar{f} \quad (3)$$

$$\rho \bar{f} = \bar{F}_b = \rho_c \bar{E} \quad (4)$$

Here, $\bar{V}$ is the velocity field, ρ is the fluid density, P is the pressure, μ is the dynamic viscosity and $\rho \bar{f}$, shown in Eq. (4), is the body force per unit volume of plasma created by the plasma actuator [1], [2], [4]. (An example of the UDF used in this study can be seen in the appendix along with the procedure for linking the UDF to the flow solver.) In this relation, ρ_c is the charge density and $\bar{E}$ is the electric field produced by the plasma actuator. The momentum source magnitude is directly proportional to the power required by the actuator.

This source term was restricted to the area designated as the location and size of the plasma region of the actuator. Experiments ([3], [4]) have shown that the actuator electrodes can be comprised of thin foil tape and for electrodes in an asymmetric configuration, the size of the plasma region is approximately the same height or thickness as the exposed electrode. However the length of the plasma is highly depended on the ambient conditions in that as the pressure decreases, the length of the plasma produced by the actuator increases in the chord wise direction. This has been demonstrated through experimental by Nichols and Rovey [19]. For this analysis, the length of the plasma region was taken to be the same length as the embedded electrode. These dimensions were chosen to be 10 mm long by 0.1 mm thick to represent the relative size of the foil tape used in previous experiments.

To model the unsteady actuator, simple alterations to the UDF had to be made to account for the time dependent fluctuation of the plasma actuator. The actuator time dependency, or rather the actuation period and frequency, were based on the physical frequency given by the Strouhal number, shown in Eq. (5) where L_{sep} is the length of the separation region and U_∞ is the free-stream velocity.

$$St = \frac{fL_{sep}}{U_\infty} \tag{5}$$

It has been shown that the optimum actuator frequency, f, occurs when the Strouhal number is near unity [3], [4], [7], [9]. After solving Eq. (5) for the frequency, a fundamental period can be determined using Eq (6).

$$T_f = \frac{1}{f} \tag{6}$$

This fundamental period can also be regarded as one actuation period. The fraction of this period that the actuator is operating is known as the duty cycle. For instance, if the duty cycle is equal to 1, this implies that there is no unsteady period during the operation of the actuator over one fundamental actuator period; or rather, this would be a steady actuator. On the other hand, if the duty cycle was 0, there would be no actuation over the fundamental period; or rather, the actuator would be in the off position. The relationship between the duty cycle, D, and fundamental period is shown in Eq. (7), where T denotes the period that the actuator is on during one fundamental period. This is shown graphically in Figure 2.5.

$$D = \frac{T}{T_f} \tag{7}$$

The duty cycle can also be interpreted another way. In terms of power, the duty cycle represents the power usage of an unsteady plasma actuator, compared to an actuator in steady operation. For example, an actuator operating with a 10% duty cycle uses 90% less power than a steady actuator over the same time period. For this study, a duty cycle of 50% was used for the unsteady actuator analysis as this has been shown to be adequate for aerodynamic control applications [9].

For design purposes, it is necessary to determine the input voltage and frequency of the plasma actuators used in this study. As the input into the UDF is a force per unit volume and the dimensions of the plasma region are specified, a relationship is needed to determine such information.

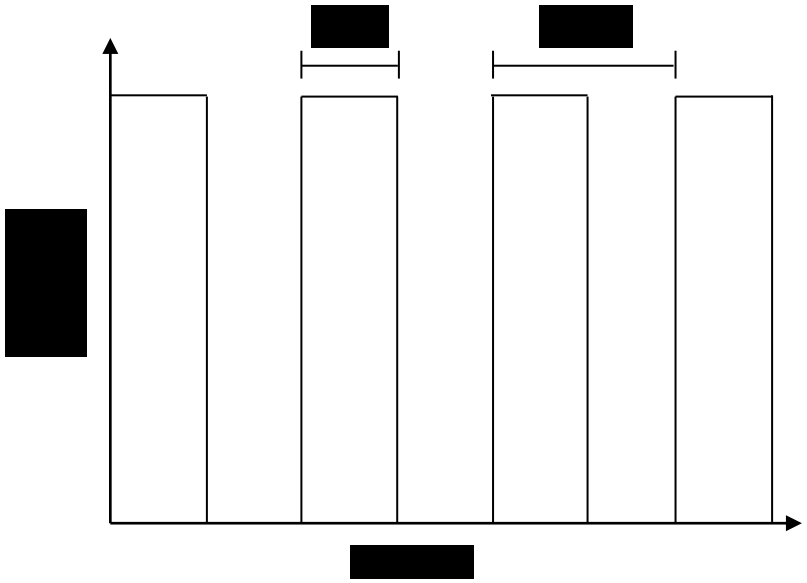

Figure 2.5: Unsteady Actuator Duty Cycle

Porter et al. [14] performed an experiment to develop relationships between the force per unit length and the input frequency and voltage. In this study, the results are presented in correspondence with a fixed input frequency of 5 kHz, and a linear relationship between the force per unit span of the actuator and the input voltage. The force per unit span changes with the input voltage using Eq. (8).

$$F_B = 3.26\,V - 17.32 \tag{8}$$

Here, F_B is in mN/m V is in kV. This approximation should be sufficient for providing insight into the requirements for a physical system that utilizes plasma actuators in the manner demonstrated in this study. Note that frequency of the unsteady operation of the actuator is much less than the operational frequency of the actuator. In this study, the highest frequency analyzed was only 20 Hz, where the assumed operational frequency of the actuator is 5 kHz.

3. LAMINAR SEPARATION CONTROL

In this portion of the study, two angles of attack, 8 and 10 degrees, were analyzed. The purpose for analyzing two angles of attack is to illustrate how performance of the plasma actuators used for 8 degrees changes at 10 degrees. Increasing the angle of attack from 8 to 10 degrees moves the separation location closer to the leading edge of the airfoil. Along with this, the magnitude of the adverse pressure gradient increases making the separation more pronounced and decreasing the fluid recovery time (i.e. the time it takes for the nominal flow to recover from a perturbation.) At 10 degrees, the formation of a laminar separation bubble still occurs. However, the separation bubble, in this case, is smaller in terms of physical dimensions due to the reduced length over which the detached laminar boundary layer has to grow before the transition to turbulent flow forces reattachment.

Three plasma actuators located at 2, 4 and 6 percent of the chord length were analyzed with varying body force magnitude, or rather, voltage input. (Recall that the input frequency is fixed at 5 kHz for the experimental relationship used.) The minimum voltage used was 5.62 kV which corresponds to a force of 1 mN/m. Porter et al. [14] noted that there is a threshold voltage where no plasma is generated. The minimum voltage used in this portion of the study is just above the threshold of 5.31 kV. Table 3.1, Table 3.2, Table 3.3 and Table 3.4 give the results for the lift to drag ratios (L/D) of the performed parametric study at 8 and 10 degrees angle of attack. The parameters were the actuator configuration (single or multiple), operation mode (steady or unsteady) and the input voltage.

Table 3.1: Parametric L/D Results for Laminar Separation Bubble Control at 8 Degrees Angle of Attack with a Single Plasma Actuator

8 Degrees	Actuator Location (% chord)		
V (kV), Duty Cycle	2	4	6
No Actuator	21.91	21.91	21.91
5.62, D=50%	30.31	22.72	21.81
5.62, Steady	27.09	22.70	21.71
5.93, D=50%	32.32	25.98	22.06
5.93, Steady	29.33	24.96	21.92
6.54, D=50%	32.65	32.57	23.38
6.54, Steady	30.89	31.67	31.36

Table 3.2: Parametric L/D Results for Laminar Separation Bubble Control at 8 Degrees Angle of Attack with Multiple Plasma Actuators

8 Degrees	Actuator Location (% chord)		
V (kV), Duty Cycle	2 and 4	2 and 6	4 and 6
No Actuator	21.91	21.91	21.91
5.62, D=50%	31.16	30.85	22.79
5.62, Steady	29.69	27.55	22.76
5.93, D=50%	32.69	32.55	31.14
5.93, Steady	31.11	31.28	31.4

Table 3.3: Parametric L/D Results for Laminar Separation Bubble Control at 10 Degrees Angle of Attack with a Single Plasma Actuator

10 Degrees	Actuator Location (% chord)		
V (kV), Duty Cycle	2	4	6
No Actuator	19.40	19.40	19.40
5.62, D=50%	20.89	20.51	19.86
5.62, Steady	21.61	21.19	20.02
5.93, D=50%	23.51	21.30	20.19
5.93, Steady	27.26	22.37	20.62
6.54, D=50%	30.45	22.52	20.90
6.54, Steady	30.99	24.51	21.78
7.77, D=50%	32.65	24.62	22.17
7.77, Steady	31.12	27.99	23.72

Table 3.4: Parametric L/D Results for Laminar Separation Bubble Control at 10 Degrees Angle of Attack with Multiple Plasma Actuators.

10 Degrees	Actuator Location (% chord)		
V (kV), Duty Cycle	2 and 4	2 and 6	4 and 6
No Actuator	19.40	19.40	19.40
5.62, D=50%	21.67	21.02	20.76
5.62, Steady	23.67	22.28	21.55
5.93, D=50%	24.24	23.04	21.67
5.93, Steady	29.61	28.36	23.03
6.54, D=50%	30.97	30.18	23.24
6.54, Steady	30.34	30.10	25.42

3.1. INVESTIGATION OF FLOW CONTROL WITH A SINGLE, STEADY ACTUATOR

The first scenario analyzed involved the use of a single, steady-state actuator. The three actuators were operated at two different input voltage levels to illustrate the effect of the strength of the body force on LSB control. Pressure coefficient contours with stream traces on the upper surface in the vicinity of leading edge are shown in Figure 3.1.

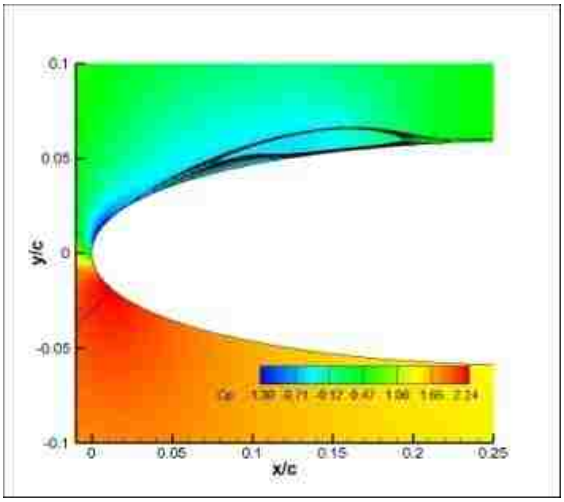

a) No Actuator

Figure 3.1: Pressure Coefficient Contours with Streamlines of One Steady State Actuator at 8 Degrees Angle of Attack. V = 5.93 kV Left, V = 6.54 kV Right (V = Input Voltage with 5 kHz Input Frequency)

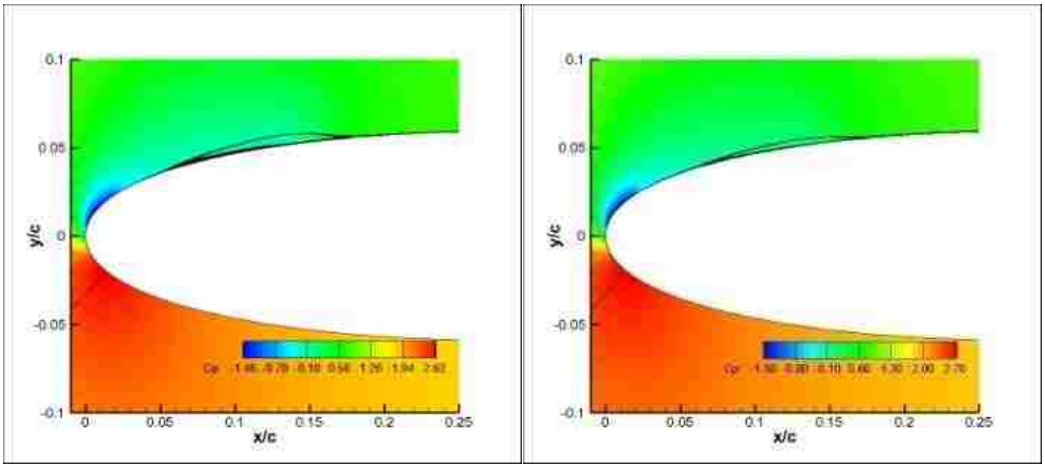

b) 2% Chord Actuator

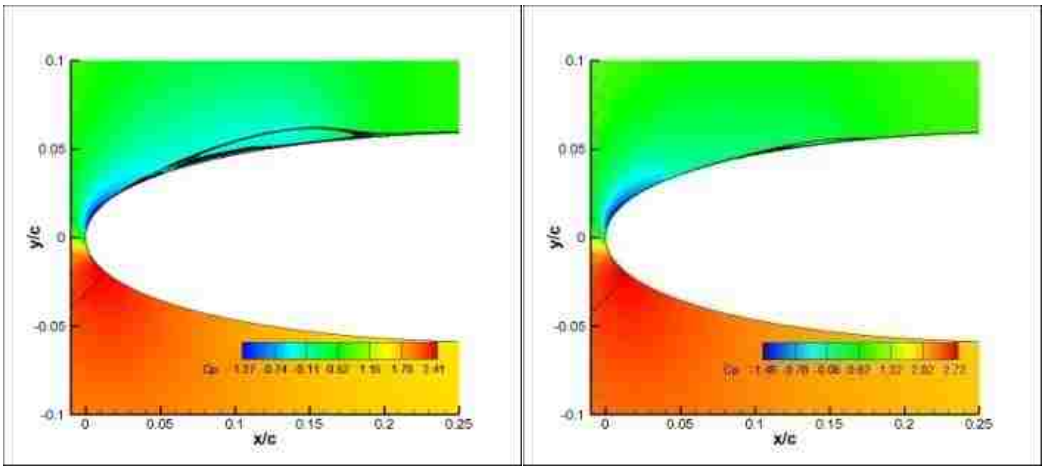

c) 4% Chord Actuator

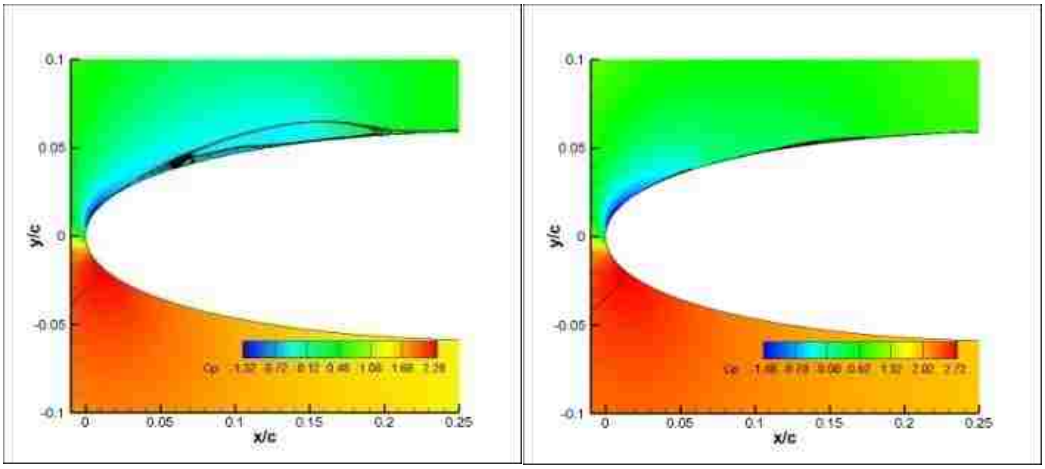

d) 6% Chord Actuator

Figure 3.1: Pressure Coefficient Contours with Streamlines of One Steady State Actuator at 8 Degrees Angle of Attack. V = 5.93 kV Left, V = 6.54 kV Right (V = Input Voltage with 5 kHz Input Frequency) (cont.)

For the case with no actuator at 8 degrees angle of attack, from Table 3.1, the lift to drag ratio (L/D) was about 21.91. By inspection of Figure 3.1, it can be seen that the plasma actuator has the ability to drastically reduce the size of the separation region. Evaluation of the L/D results in Table 1 shows that there is as much as a 45% improvement in L/D when using a single, steady actuator. This is a significant improvement in aerodynamic performance. The reduction in the size of the separation region allows for a decrease in pressure drag as well as in improvement in the pressure distribution with an increase in the suction near the leading edge.

The images above also illustrate the importance of the location of the actuator. Because of the large magnitude of the source, the 6.54 kV cases appear to be independent of the actuator location. However, at the lower force level, it can be seen that as the actuator moves downstream, its effectiveness decreases. In fact, at the 6% chord location, the flow behaves as if there was no flow control device present at all. These results help to illustrate, physically, how the plasma actuator modifies the near-wall flow field. Because of the body force near the wall, the flow is being accelerated near the wall, preventing separation from occurring. If the actuator is placed just before the point at which the separation of the boundary layer is anticipated, then the separation can be delayed, or even prevented. On the contrary, if the actuator is placed downstream of the separation point, the flow entrainment may not be substantial enough to reattach the flow. This will be an important concept later when attempting to control the flow separation at stall conditions. For the 8 degree angle of attack case, it can be seen that the actuator located at 2% of the chord length provides the most improvement in aerodynamic performance for the lower, 5.93 kV, input. However, notice that the separation bubble is smaller for the 6.54 kV input when the actuator is located at 4% of the chord. At the higher force magnitude, the flow is being entrained near the wall, ahead of the actuator. This is preventing the separation from actually occurring until downstream of the actuator. By this time, the boundary layer only has a small time period before the transition to turbulent flow forces reattachment.

Figure 3.2 illustrates the magnitude of the pressure recovery achieved with a plasma actuator. This plot compares the surface pressure distribution of the airfoil without a plasma actuator to the case where there is one actuator located at 4% of the

chord with an input voltage of 6.54 kV. Because of the added momentum near the leading edge of the airfoil, the suction on the upper surface spikes dramatically with over a 25% increase in the pressure coefficient on the upper surface. It can be seen that for this case the actuator does not entirely eliminate the separation bubble. However, the addition of the momentum near the wall delays the separation of the boundary enough such that there is very little time for the detachment distance of the boundary layer to increase before transitioning to turbulent flow and reattaching. Overall, there is about an 8% increase in lift and a 25% decrease in drag. Actually, the decrease in drag is quite interesting. The plasma actuator causes a 50% decrease in pressure drag. This can be explained by the reduction in the size of the separation bubble. The interesting part is the skin friction drag, which actually increases over 80%. While the skin friction component of the drag is small for the uncontrolled case, when the actuator is on, the two drag components are nearly the same, as the contribution of each is about 50% of the total drag. Note that these results are only for this specific case. In the cases when the actuator does not significantly decrease the bubble size, the skin friction drag will be much less than the pressure drag component. Note that the sharp spike in Figure 3.2, on the actuator curve, is caused by the actuator.

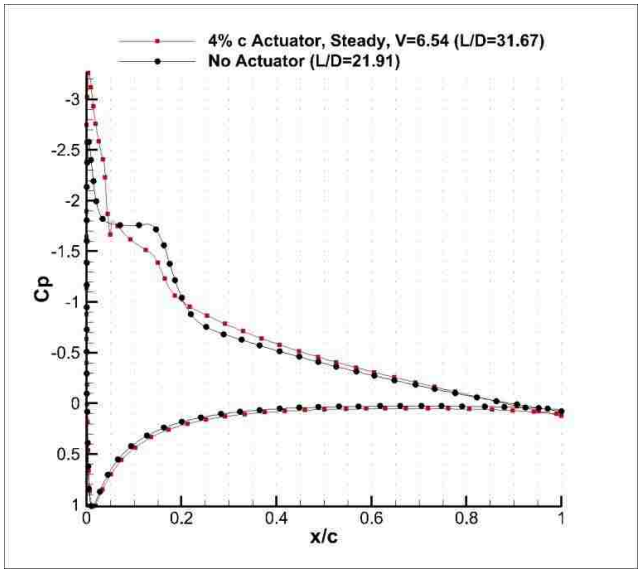

Figure 3.2: Surface Pressure Coefficient Distribution with and without a Single Plasma Actuator 8 Degrees Angle of Attack

Upon increasing the angle of attack from 8 degrees to 10 degrees, the location of the separation of the laminar boundary moves forward a distance of about 1% of the chord. The pressure contours with stream traces for the three actuators at the same two voltage levels are shown in Figure 3.3.

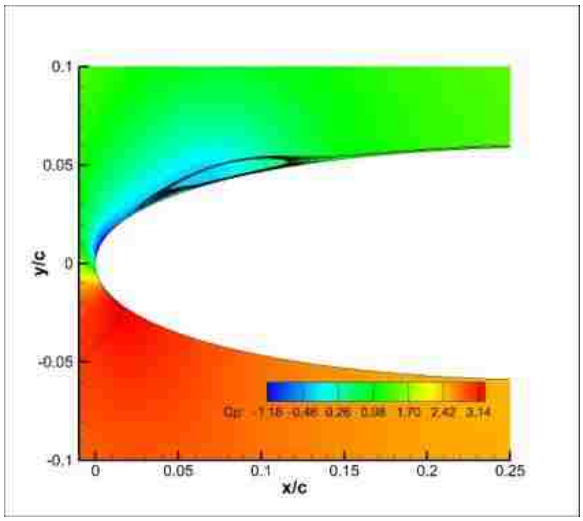

a) No Actuator

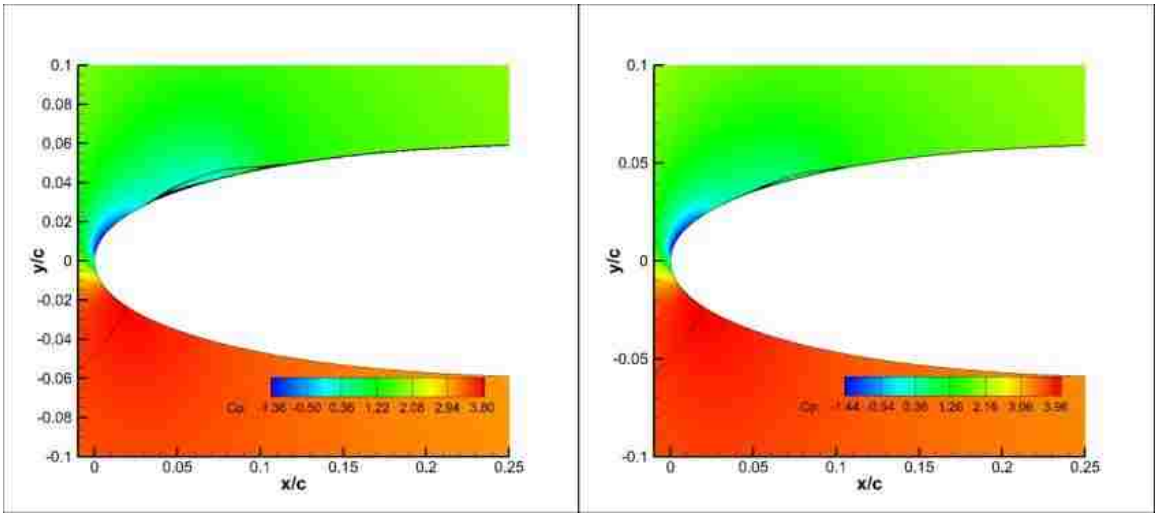

b) 2% Chord Actuator

Figure 3.3: Pressure Coefficient Contours with Streamlines of One Steady State Actuator at 10 Degrees Angle of Attack. V = 5.93 kV, Left. V = 6.54 kV, Right

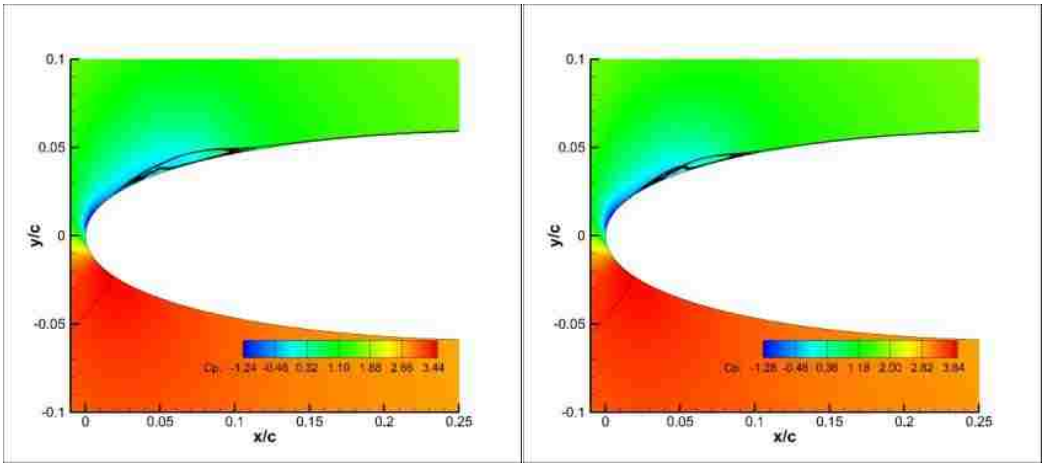

c) 4% Chord Actuator

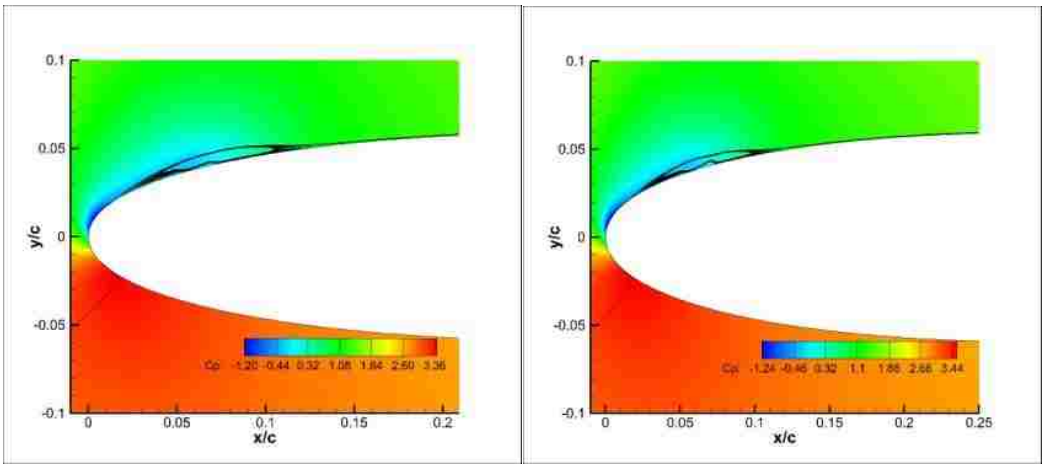

d) 6% Chord Actuator

Figure 3.3: Pressure Coefficient Contours with Streamlines of One Steady State Actuator at 10 Degrees Angle of Attack. V = 5.93 kV, Left. V = 6.54 kV, Right (cont.)

Comparing the results from the two angles of attack, it can be seen that the now instead of only the 6% actuator having very little influence on the separation bubble, the 4% actuator has greatly lost its effectiveness. This is expected as the separation bubble has propagated upstream and the 4% actuator can no longer entrain the flow enough to prevent the boundary layer from separating prior to the actuator at the same voltage levels. Note that it may still be possible to control the separation bubble with a 4% or even a 6% actuator, however this would be extremely costly in terms required voltage and, in turn, power making this an inefficient approach.

3.2. INVESTIGATION OF FLOW CONTROL WITH A SINGLE, UNSTEADY ACTUATOR

In an effort to reduce the power consumed by the actuators, another mode of operation was considered. As mentioned earlier, it has been shown that the use of an unsteady or pulsed actuator can improve aerodynamic characteristics as much as or even more than that achieved from a steady state actuator. Figure 3.4 shows a time sequence of the effect of the unsteady actuator. Here, a periodic vortex shedding process is occurring. As the laminar separation bubble is forming, it is quickly forced to separate from the surface before developing into a large bubble. This can be seen as a kind of bursting effect. Due to the similarity between the scenarios involving unsteady actuators, only one example is given. As long as the vortex shedding is present, all that changes between different actuator configurations and strengths is the size of the vortex that is shed. This means that a larger vortex will result in a greater loss in aerodynamic performance, but still may be better than a scenario where no control is present. This is evident in Figure 3.5. Because the drag is not as low for the 4% chord actuator compared to the 2% chord actuator, this suggests that the vortex being shed is larger than in the 2% chord actuator. Note that in some cases, the actuator may have little or no effect on the separation region, as with the 6% chord actuator in Figure 3.5. Similar to the steady actuators, this is due to the actuator placement with respect to the separation location. In fact, the unsteady actuators are actually more dependent upon the placement as pulsing the actuator reduces the upstream influence of the actuator that was seen for the steady operation. This indicates that the placement of the plasma actuator is crucial, in that is must be located just upstream of the point of separation for the most efficient and effective flow control.

Flow Time = 8 sec. *Flow Time = 10 sec.*

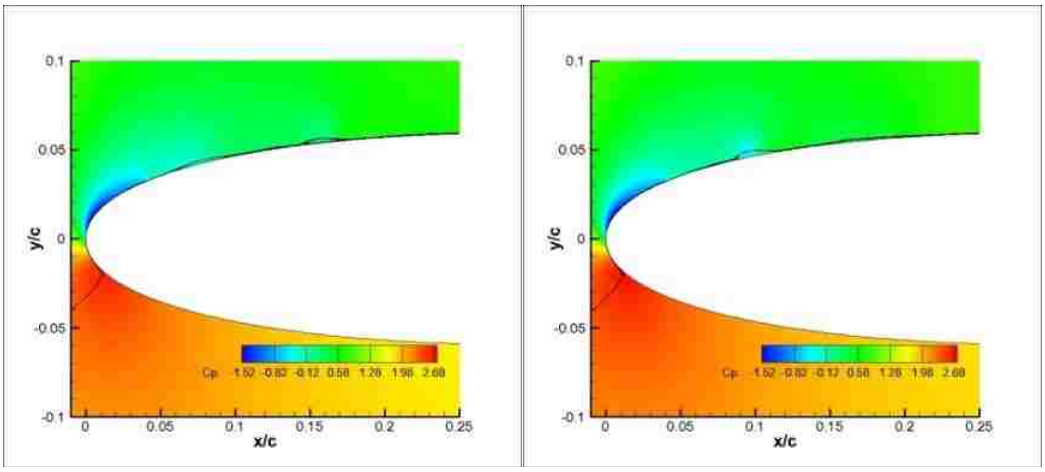

Flow Time = 12 sec. *Flow Time = 14 sec.*

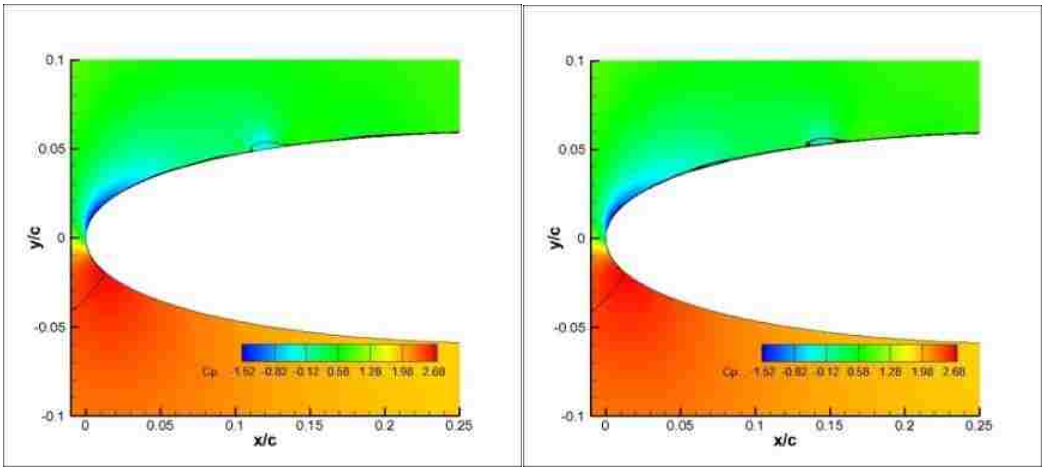

Flow Time = 16 sec. *Flow Time = 18 sec.*

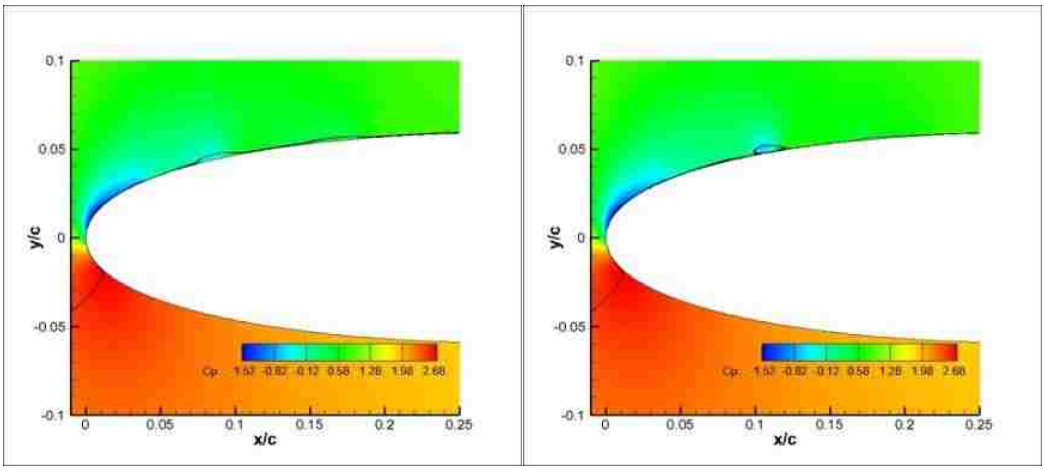

Figure 3.4: Pressure Coefficient Contours with Streamlines at 8 Degrees Angle of Attack with One Unsteady Actuator at 4% c. V = 6.54 kV kV, D = 50%

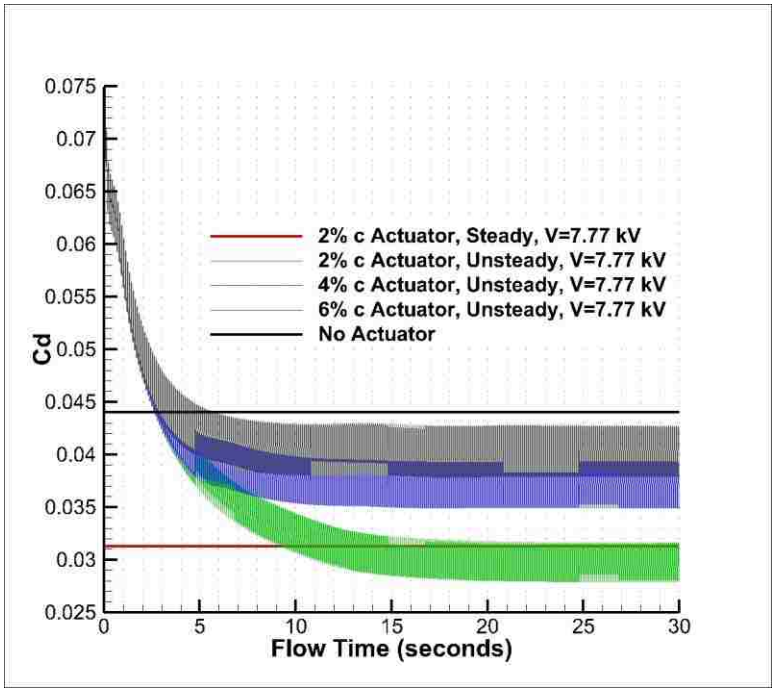

Figure 3.5: Drag Coefficient vs. Flow Time for Single Unsteady Actuators at 10 Degrees Angle of Attack. V = 7.77 kV, D = 50%

3.3. INVESTIGATION OF FLOW CONTROL WITH MULTIPLE, STEADY ACTUATORS

Multiple actuators may offer a substantial gain in efficiency and control potential over a single actuator. It has already been shown that as the angle of attack increases, the separation location propagates upstream. From the single actuator results, it has been shown that an actuator downstream of the separation location may have little to no control over the separation region. Figure 3.6 shows the results of using two steady state actuators at 8 degrees angle of attack. Here, the actuators were being operated at lower input voltages than that of the single actuator cases, as this is one of the goals of using multiple actuator systems. Note that the same three actuators are still in use (2, 4 and 6% chord), and all possible combinations have been considered.

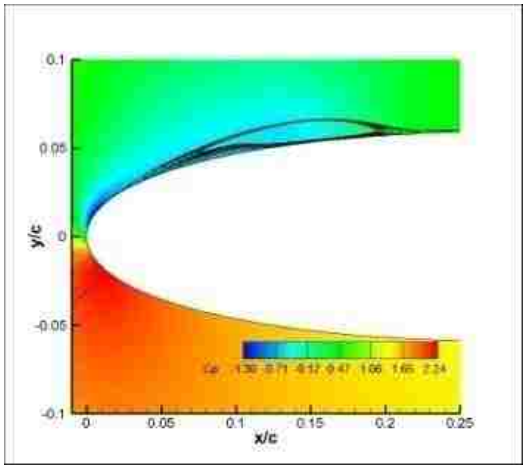

a) No Actuator

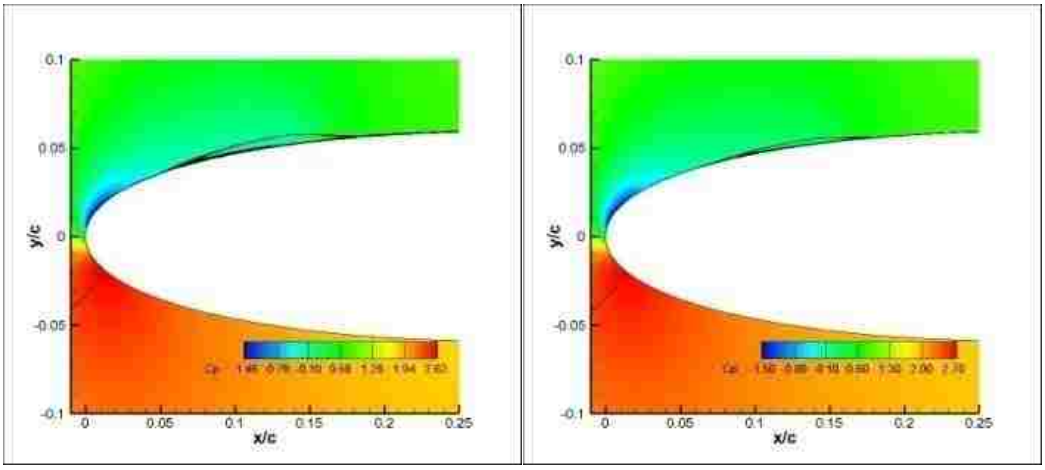

b) 2 and 4% Chord Actuators

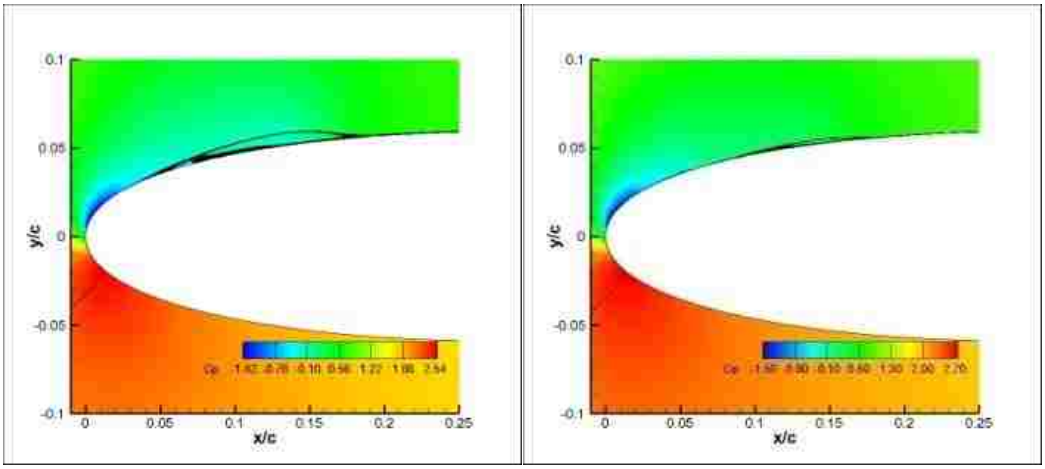

c) 2 and 6% Chord Actuators

Figure 3.6: Pressure Coefficient Contours with Streamlines of Two Steady State Actuators at 8 Degrees Angle of Attack. V = 5.62 kV each, Left. V = 5.93 kV each, Right

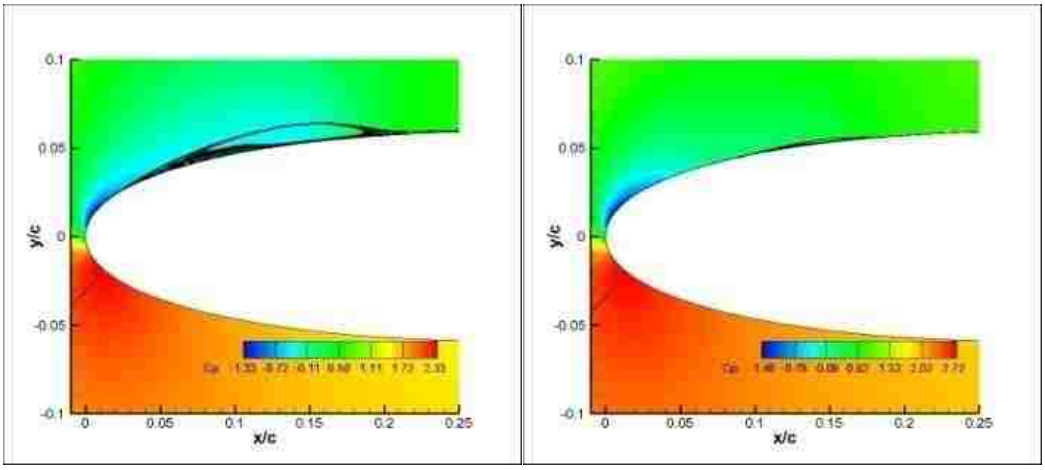

d) 4 and 6% Actuators

Figure 3.6: Pressure Coefficient Contours with Streamlines of Two Steady State Actuators at 8 Degrees Angle of Attack. V = 5.62 kV each, Left. V = 5.93 kV each, Right (cont.)

As with the single actuator, the effects of the surface body force can be observed from the stream traces above. The separation point is pushed downstream, reducing the size of the separation bubble. With the multiple steady actuators, the total body force acts as if it were an additive resultant from the two actuators. In general, if the actuators are close together, as in these cases, this statement will likely hold true. It may actually be difficult to discern between using one actuator or two, especially in the case when the fluid recovery time is large enough that no separation occurs between the actuators.

Figure 3.7 shows the results for two steady state actuators at 10 degrees angle of attack. The results are quite different from 8 degrees. The separation region carries more energy at the 10 degrees. In turn, at the lower voltage level the pair of actuators have relatively no influence. Also recall that at 10 degrees angle of attack the fluid recovery time is significantly less compared to 8 degrees. This allows for the flow separate only a short distance past the actuator. When there is an actuator at 2% c, the separation is slightly delayed; however the flow rapidly detaches and grows rendering the second actuator effectively useless. At the higher 5.93 kV input voltage, the 2% actuator is able to greatly reduce the separation bubble size, but the second actuator still plays little part in controlling the separation region. This is because the fluid recovery time is simply too short. In the case of actuators at 2% and 4% c at 5.93 kV, it can be seen that a small

separation region actually exists between the two actuators. Moving the actuators closer together may help to improve the capabilities of multiple actuators when the effect of the actuator is quickly dissipated.

Furthermore, notice that in the cases with the 4% and 6% actuator the actuators have little effect. There is some distortion in the bubble structure due the added momentum, however the bubble simply passes over the actuators as, again, their influence does not reach very far downstream for the selected input voltage levels. This is not to say these actuators are ineffective, as with a high enough input voltage, this particular configuration could effectively control the flow, just not efficiently. The ineffectiveness of these actuators also reaffirms the importance of actuator placement for effective and efficient control of separated flows.

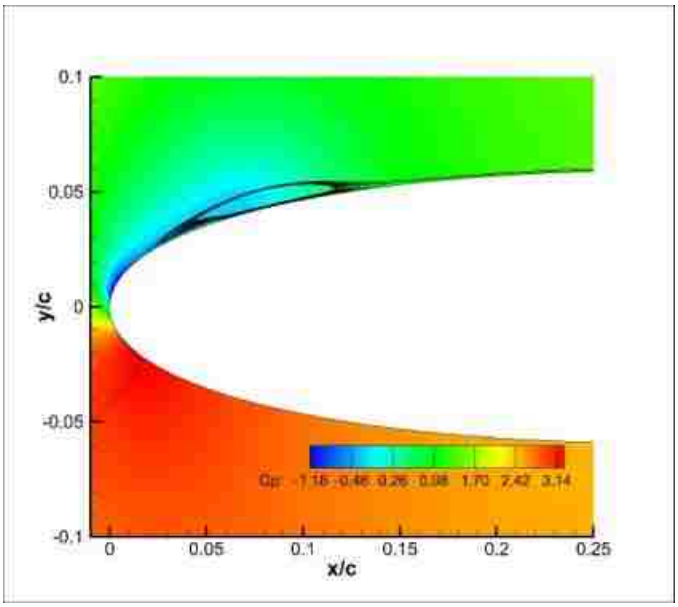

a) No Actuator

Figure 3.7: Pressure Coefficient Contours with Streamlines of Two Steady State Actuators at 10 Degrees Angle of Attack. V = 5.62 kV each, Left. V = 5.93 kV each, Right

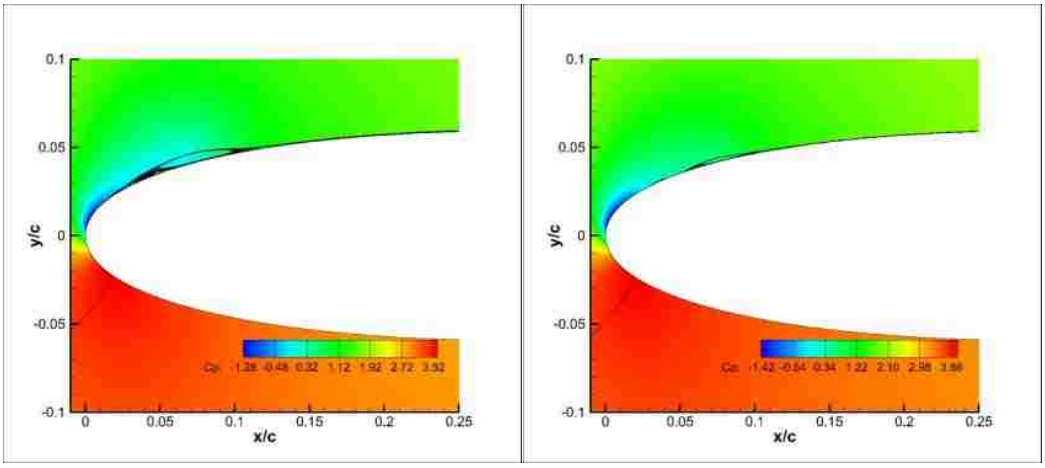

b) 2 and 4% Chord Actuators

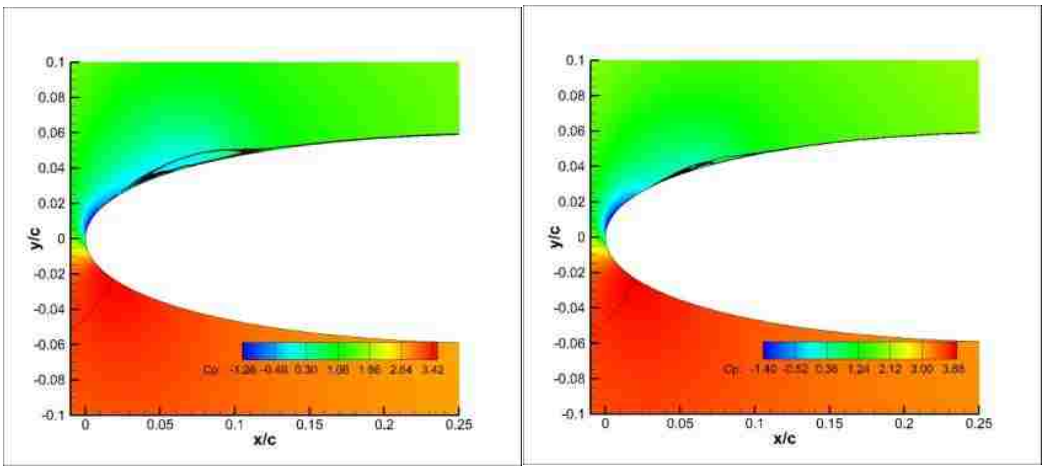

c) 2 and 6% Chord Actuators

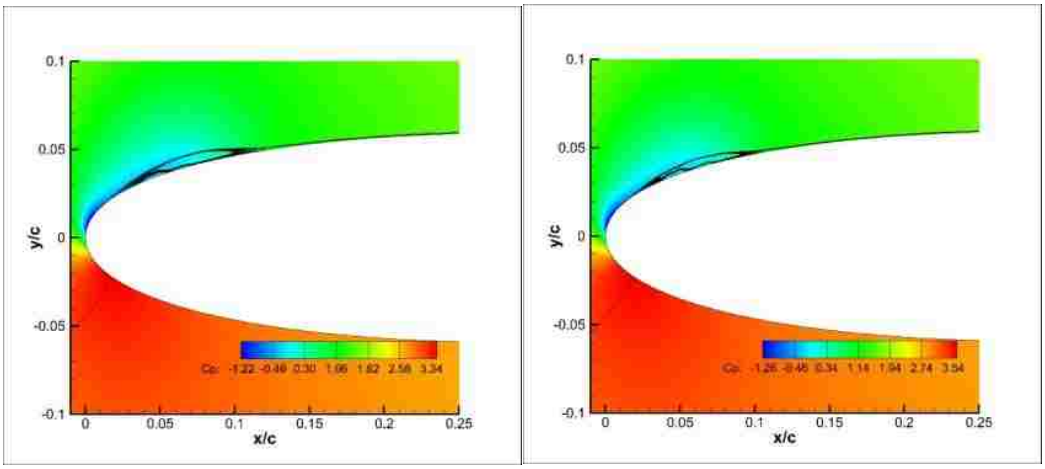

d) 4 and 6% Actuators

Figure 3.7: Pressure Coefficient Contours with Streamlines of Two Steady State Actuators at 10 Degrees Angle of Attack. V = 5.62 kV each, Left. V = 5.93 kV each, Right (cont.)

3.4. INVESTIGATION OF FLOW CONTROL WITH MULTIPLE, UNSTEADY ACTUATORS

Using the same actuator configurations as in the steady state multiple actuator cases, the actuators could be operated in an unsteady mode. Because the success of the single unsteady actuator, it was expected that similar improvement would be seen for multiple unsteady actuators. Recall that in the case of multiple unsteady actuators, they are operated just out of phase. Because of the 50% duty cycle used in this study, there will always be one actuator operating at a given time. For the 8 degree angle of attack case, multiple, unsteady actuators provide nearly the same aerodynamic improvement as the cases with a single, unsteady actuator with the same power consumption over the same period of time. Because the actuators are so close together, the fluid behaves as if there is one steady actuator present on the surface of the airfoil. With a single, more powerful actuator, the influence of the actuator reaches nearly the same distance downstream as the two unsteady actuators at a lower power level and gives the impression of steady actuation. This holds true because there is no separation occurring between the actuators. However this is only true at this angle of attack in which the fluid recovery time is quite long relative to 10 degrees angle of attack.

At 10 degrees, the same trend is not observed. At the same force levels as at 8 degrees, the multiple unsteady actuator configurations are not nearly as effective as a single, unsteady actuator. This is because the flow recovers too quickly after the first "push" from the upstream actuator and begins to separate before reaching the downstream actuator making the downstream actuator relatively ineffective. However, note that this is only the case when the force level is the same as in the 8 degree cases. Increasing the force magnitude (a higher input voltage) would allow the upstream actuator to give enough of a "push" such that the flow stays attached through both actuators, without separation between.

Note that for cases involving multiple, unsteady actuator configurations the same vortex shedding phenomenon is in place as seen in the cases with a single, unsteady actuator. Figure 3.8 shows an example of this at 8 degrees angle of attack as compared to having no actuator and a single, steady actuator of with the same time averaged body force magnitude. Notice that the 4 and 6% actuator chord array has a significantly higher

drag. As with the single, unsteady actuator cases, this is because the size of the vortex being shed is much larger than the other two configurations. Similar to all of the other actuator configurations discussed, this is related to the placement of the actuators with respect to the separation region. The 4 and 6% actuators lie inside the separation region and, with an input voltage of 5.62 kV each, the flow is not being entrained enough to prevent separation from occurring upstream of the 4% actuator. Due to the unsteadiness caused by the pulsing actuators, the described vortex shedding process is in place. However, in this case, only a portion of the separation bubble is being shed. The initial separation upstream of the 4% actuator is not being prevented or even suppressed.

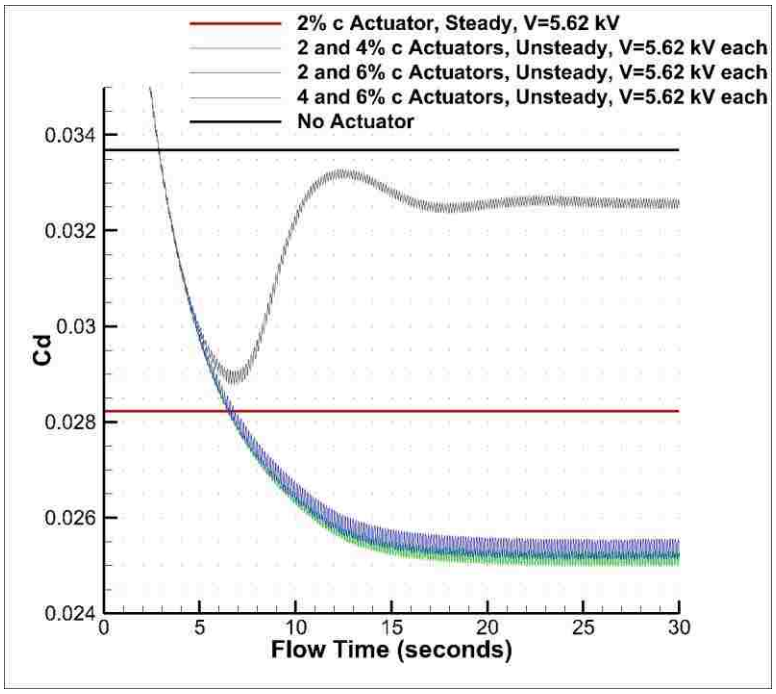

Figure 3.8: Drag Coefficient vs. Flow Time for Multiple Unsteady Actuators at 8 Degrees Angle of Attack. V = 5.62 kV each, D = 50%

3.5. SUMMARY OF THE RESULTS

3.5.1. Plasma Actuator Location. Several conclusions can be drawn from these results. The first is related to the importance of the actuator location. For the lower powered steady state actuators and all of the unsteady actuator arrangements, actuator

placement dominates the effectiveness of the actuator(s). The actuator must be located just upstream of the separation location in order to have a substantial influence on the separation bubble. This is true for both angles of attack. Here in lies that advantage/need of using multiple actuator systems. In this study, only two angles of attack are examined, however if the angle of attack was reduced to five or six degrees, the separation location would be downstream enough that the 2% chord actuator may now be ineffective, and the 6% chord or even a further downstream actuator would be ideal.

3.5.2. Steady vs. Unsteady Plasma Actuators. A second conclusion that can be made is with regards to the use of unsteady actuators. Because the critical factor in implementing plasma actuators as a feasible, active flow device will likely be the power usage, it is critical to reduce power consumption in any way possible. This is where the use of unsteady actuators show significant promise. From Table 3.1 notice that for a 6.54 kV, steady actuator at the 2% chord location, L/D = 30.98 whereas with a 5.93 kV, unsteady actuator (D = 50%) at the 2% chord location, L/D = 32.32. This is an improvement over the steady actuator at 25% of the body force magnitude, which is synonymous to 25% of the power required. It can be seen from both Tables 3.1 and Table 3.3 that, in general, unsteady actuators always outperform steady actuators at the same time averaged body force magnitude, but not always at the same force input. For example, from Table 3.3, notice that for a 6.54 kV input, the steady actuator has an L/D = 30.99, but the unsteady actuator with the same input has an L/D = 30.45. However, the unsteady actuator is using exactly half of the power as the steady actuator. The same power as this unsteady actuator is also used by the 5.93 kV steady actuator. Notice that the unsteady actuator out performs the steady actuator at the same time averaged body force or power input.

3.5.3. Effect of Multiple Plasma Actuators. Lastly, the use of multiple actuators can yield significant improvements over single actuators at a much lower power requirement in some cases, but not all. The primary advantage of the multiple actuators is that, because of the dependence on the placement of the actuator, multiple actuators can give a wider range of control. It can be shown that as the angle of attack increases, the separation point advances forward. If an aircraft is designed with only one actuator at the 4% chord location, this actuator, in all likelihood, will not be able to effectively

control the separation region with reasonable power inputs. In the other direction, if the angle of attack were to decrease, the separation point may move downstream, and if the aircraft only has a 2% chord actuator onboard, it again may be ineffective as the added momentum from the actuator only has a short downstream influence before the added momentum is dissipated. Using multiple actuators will allow for control over a range of angles of attacks. In terms of power usage, the multiple actuators do not provide much advantage. Nearly the same aerodynamic performance enhancement can be achieved using a single actuator at the same time averaged force magnitude and operational model (steady or unsteady.) This is because of the spacing of the actuators. The actuators used here are close together, which is necessary because of the size of the studied separation region. Multiple actuators would likely prove to be beneficial in cases when separation needs to be continuously delayed over a long region. In this case, a single actuator upstream of some initial separation point may require a significantly large power input (i.e., beyond the practical limits) to maintain attached flow over some length whereas using multiple, much low powered actuators may provide a much more efficient alternative. Regardless, the same trend still holds true that, as with the single actuators, unsteady operation outperforms steady operation given the same time average body force magnitude.

4. CONTROL OF TURBULENT FLOW SEPARATION AT STALL CONDITIONS

In this portion of the study, 15 degrees angle of attack was the angle of interest. At the selected Reynolds number (100,000) used in this study, 14 degrees was the highest achievable angle of attack after which substantial separation and stall conditions were observed. At this angle, only a small region of trailing edge separation exists, which has little effect on the aerodynamic performance of the airfoil. At 15 degrees, the separation proceeds to cover nearly the entire upper surface of the airfoil which severely compromises its lift and drag characteristics.

It is important note the type of separation observed for the NACA 0012 airfoil and flow conditions used in this study. It has been determined, by observation of the transient data associated with the uncontrolled case at 15 degrees angle of attack, that the flow separation originates in the trailing edge region. It will be shown that even after pushing the trailing edge separation back downstream with plasma actuation, this small leading edge separation bubble still remains, which appears to be stable in time.

Control of trailing edge separation may be different than what has been studied in previous literature as most of those cases focus on the control of leading edge separation with actuators placed in the leading edge region. The primary objective of the turbulent separation control investigated in this study is to force the separation region downstream as far as possible (i.e., to reduce the extent of the size of the separation region). Just moving the separation back past the maximum thickness of the airfoil will greatly improve the suction on the upper surface of the airfoil which enhances the lift. An improvement in the drag will come from forcing the separation region as far downstream as possible. Reduction of the separation zone size greatly improves the pressure drag on the airfoil, but increasing the body force magnitude to reduce the separation zone size also increases the skin friction drag. However, at the stall condition, the pressure drag component is significantly larger than the skin friction drag component making the increase in skin friction drag due to the addition of momentum near the wall negligible.

Table 4.1 and Table 4.2 give the results of the performed parametric study. Note that the parameters were the same as in the previous chapter. Also, the same 2, 4 and 6%

chord actuators used in the previous chapter are used in this portion of the study with all of the same actuator configurations. However, the minimum voltage analyzed is higher than in the LSB control study. In this chapter, a minimum voltage of 7.77 kV was used as this is the voltage where flow control with either a single steady or unsteady actuator was not possible. This is shown in Table 4.1. At the lowest voltage, the single, unsteady actuator cannot suppress the separation region.

Table 4.1: Parametric L/D Results for Turbulent Stall Separation Control at 15 Degrees Angle of Attack with a Single Plasma Actuator

15 Degrees	Actuator Location (% chord)		
V (kV), Duty Cycle	2	4	6
No Actuator	3.18	3.18	3.18
7.77, D=50%	3.95	3.23	3.20
7.77, Steady	15.73	12.30	11.30
10.22, D=50%	14.47	12.24	11.61
10.22, Steady	20.92	16.52	15.17
15.13, D=50%	18.76	15.90	15.56
15.13, Steady	25.85	20.84	19.24

Table 4.2: Parametric L/D Results for Turbulent Stall Separation Control at 15 Degrees Angle of Attack with Multiple Plasma Actuators

15 Degrees	Actuator Location (% chord)		
V (kV), Duty Cycle	2 and 4	2 and 6	4 and 6
No Actuator	3.18	3.18	3.18
7.77, D=50%	14.83	14.30	12.09
7.77, Steady	18.59	18.43	15.09
10.22, D=50%	20.03	19.23	15.83
10.22, Steady	22.30	22.64	18.30

4.1. INVESTIGATION OF FLOW CONTROL WITH A SINGLE, STEADY ACTUATOR

Figure 4.1 shows the pressure coefficient contours with streamlines for the cases with a single plasma actuator. It is important to note that the input voltage for these cases is as much as 4 times higher than what was used as the highest voltage for the laminar separation bubble cases. This is expected and the separation at this angle of attack is larger, stronger, and much more stable making it more resistant to perturbations. From the images in Figure 4.1, the effect of the actuator on the separation region can clearly be seen. The momentum added to the flow from the actuator forces the separation region downstream towards the trailing edge, reducing its size. For the case with no actuator, L/D = 3.18, as given is Table 4.1. From Table 4.1, even the worst case below (6% chord actuator with V = 7.77 kV) gives great improvement to the aerodynamic performance of the airfoil with an L/D = 11.61. This is over a 250% improvement. By forcing the separation region downstream past the maximum thickness, the suction on the leading edge increases significantly, such that the lift increases by almost 70%. The 2% chord with an input of 15.13 kV provides an L/D = 25.85 which is achieved by the massive increase in suction on the leading edge and the addition of near wall momentum that travels downstream fast enough to force the separation bubble almost completely to the tip of the airfoil.

Notice that in the cases with the input of 15.13 kV the size of the separation bubble is relatively the same between all three cases. The separation region for the 4 and 6% actuators is slightly larger, but not substantially. This might suggest that the L/D ratio is approximately the same. However, they are not as the difference between the L/D ratio of the 2% actuator is actually 35% higher than the ratio for the 6% actuator. Figure 4.2 illustrates why this is so. From this figure, notice the suction increase on the upper surface. The pressure is about 12% lower. This provides about a 6% increase in left. The remainder of the difference in the two L/D ratios then must come from the difference in drag. From the same figure, it can be seen that there is very little difference between the two cases at the trailing edge. The major difference is near the leading edge. Observing the 6% chord line, there is a hint of separation at the leading edge as the sharp increase in the pressure due the actuator is much more significant compared to the 2% chord actuator

case. This is because the 2% chord actuator is upstream of this small leading edge separation. The 2% actuator completely prevents this separation from occurring. This accounts of the nearly 22% decrease in drag from the 6% chord actuator case. The 4% chord actuator cases are all between the 2% and 6% chord actuator results. The 4% actuator is not quite upstream of the separation region and is not as effective at the 2% chord actuator.

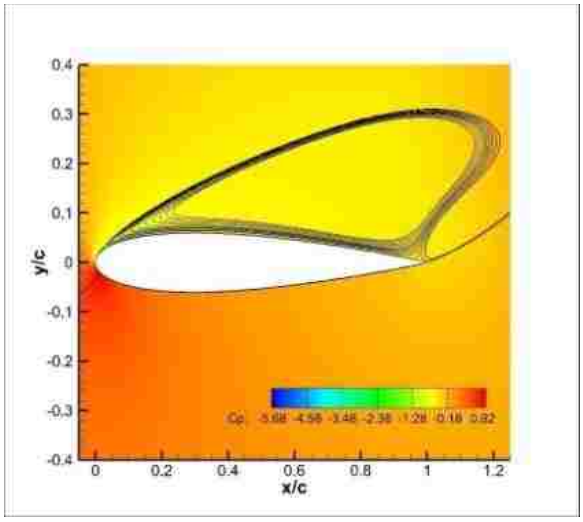

a) No Actuator

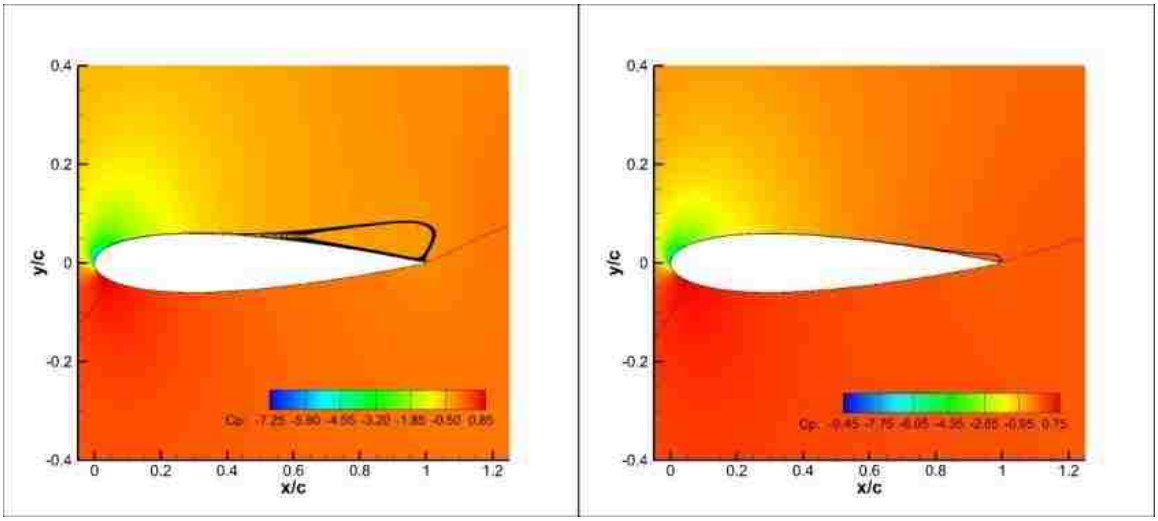

b) 2% Chord Actuator

Figure 4.1: Pressure Coefficient Contours with Streamlines of One Steady State Actuator at 15 Degrees Angle of Attack. V = 7.77 kV, Left. V = 15.13 kV, Right

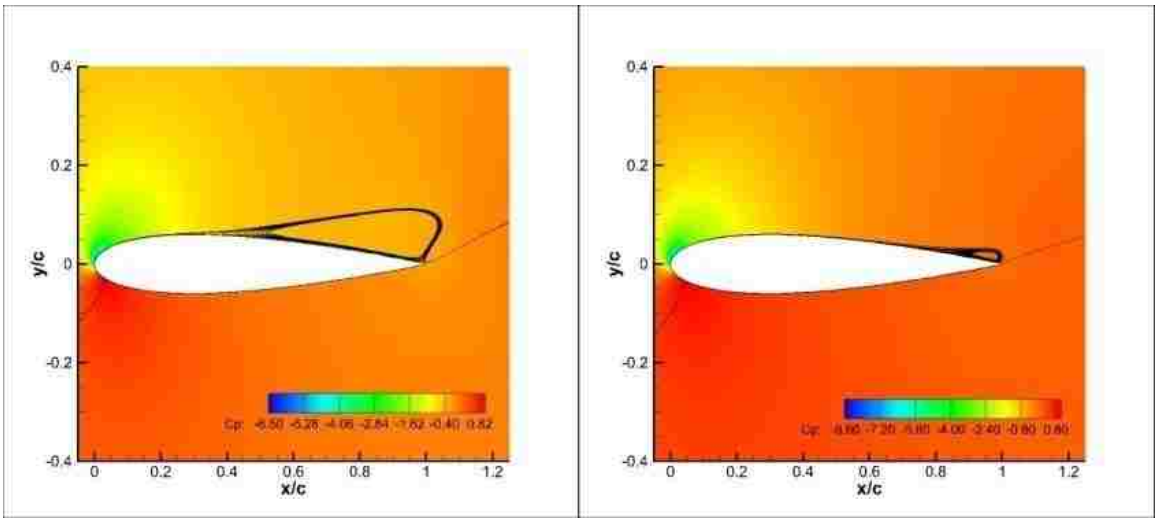

c) 4% Chord Actuators

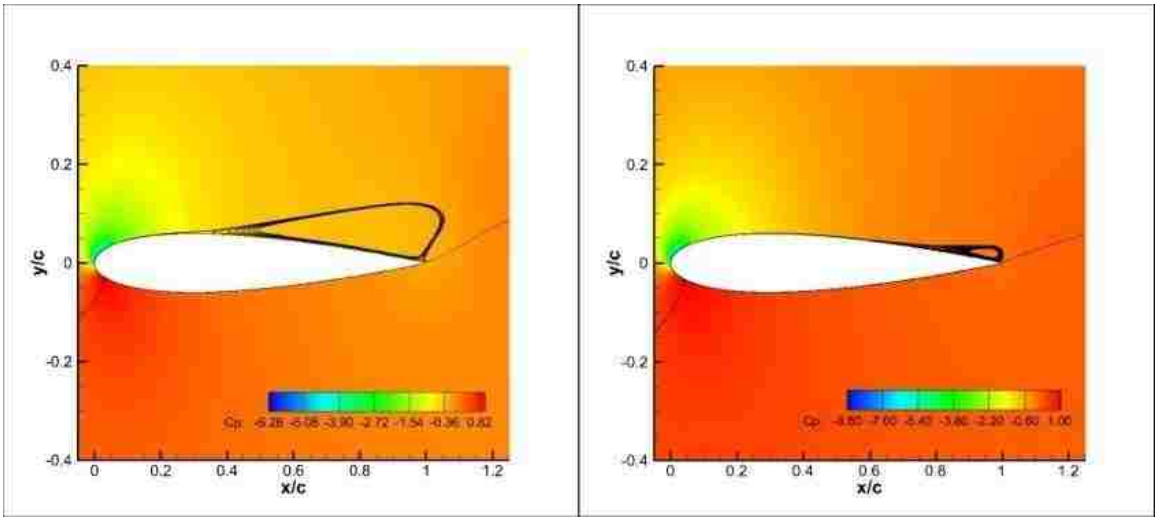

d) 6% Chord Actuator

Figure 4.1: Pressure Coefficient Contours with Streamlines of One Steady State Actuator at 15 Degrees Angle of Attack. V = 7.77 kV, Left. V = 15.13 kV, Right (cont.)

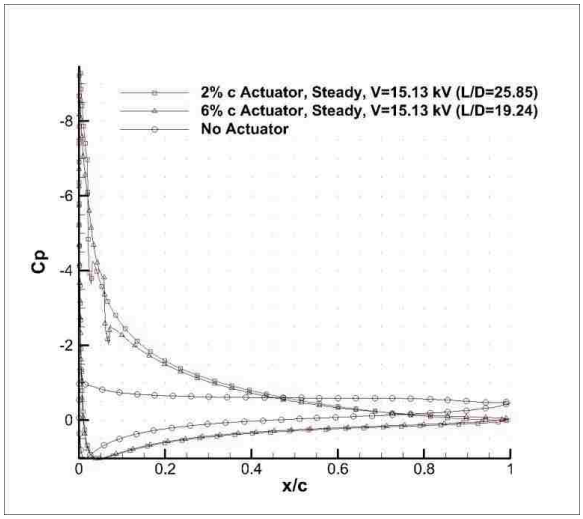

Figure 4.2: Surface Pressure Coefficient Distribution with and without a Single Plasma Actuator at 15 Degrees Angle of Attack

4.2. INVESTIGATION OF FLOW CONTROL WITH A SINGLE, UNSTEADY ACTUATOR

For a single unsteady actuator, the results are quite different when compared to the laminar separation bubble cases. Previously, the unsteady actuators induced a periodic vortex shedding process preventing the separation from growing to a stable, full size separation bubble. However, for the turbulent separation at stall conditions, this same phenomenon is not observed. Figure 4.3 shows a time sequence for a single, unsteady actuator.

Notice that the separation region never detaches from the surface of the airfoil. What is seen is the separation generated by the trailing edge swelling, then deflating with a periodic motion. Figure 4.4 shows a plot of the drag coefficient versus the flow time for this case, which confirms the behavior of the separation region. In light of this, single, unsteady actuators do not perform as well as single steady actuator. For a 2% chord unsteady actuator with a 15.13 kV input, L/D is about 12% less than a steady actuator at the same location with the same time averaged body force magnitude (V = 10.22 kV.) For all studied cases, the unsteady actuators do not perform as well as steady actuators, which is not similar to the trend observed for the control of laminar separation bubbles. This is because there is always a region of separation attached to the airfoil

surface which reduces the aerodynamic performance of the airfoil. Note, however, that there is still significant aerodynamic improvement when compared to the uncontrolled case. From Table 4.1, the greatest improvement in L/D for the cases with a single unsteady actuator was nearly 500%.

Flow Time = 25 sec. *Flow Time = 26 sec.*

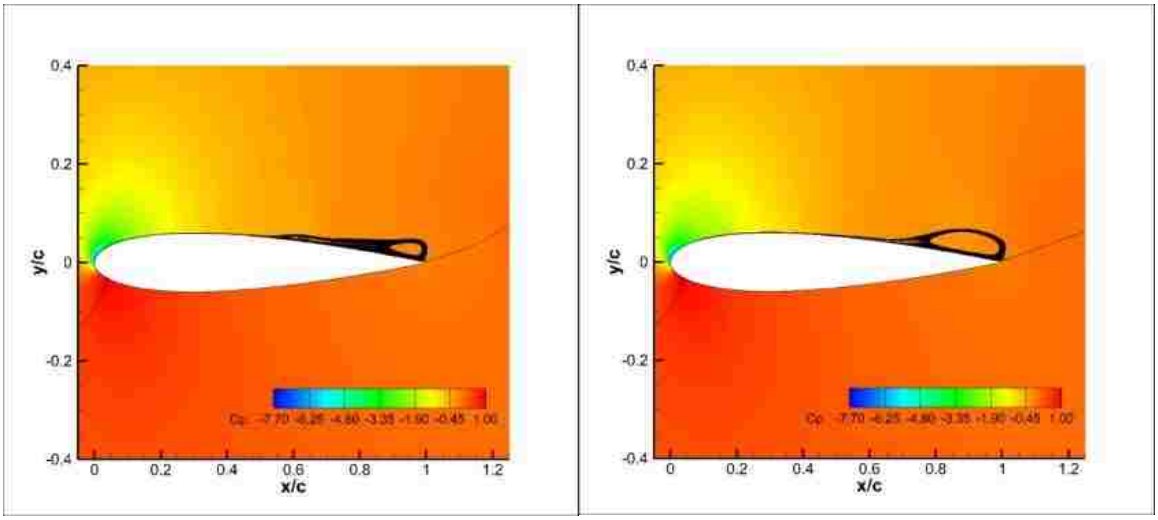

Flow Time = 27 sec. *Flow Time = 28 sec.*

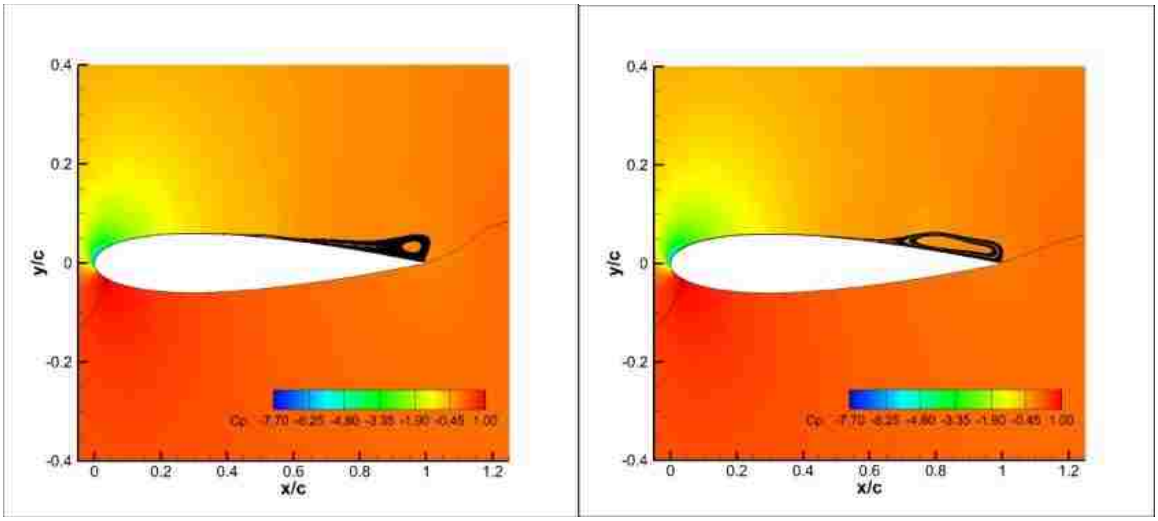

Flow Time = 29 sec. *Flow Time = 30 sec.*

Figure 4.3: Pressure Coefficient Contours with Streamlines at 15 Degrees Angle of Attack with One Unsteady Actuator at 2% c. V = 15.13 kV kV, D = 50%

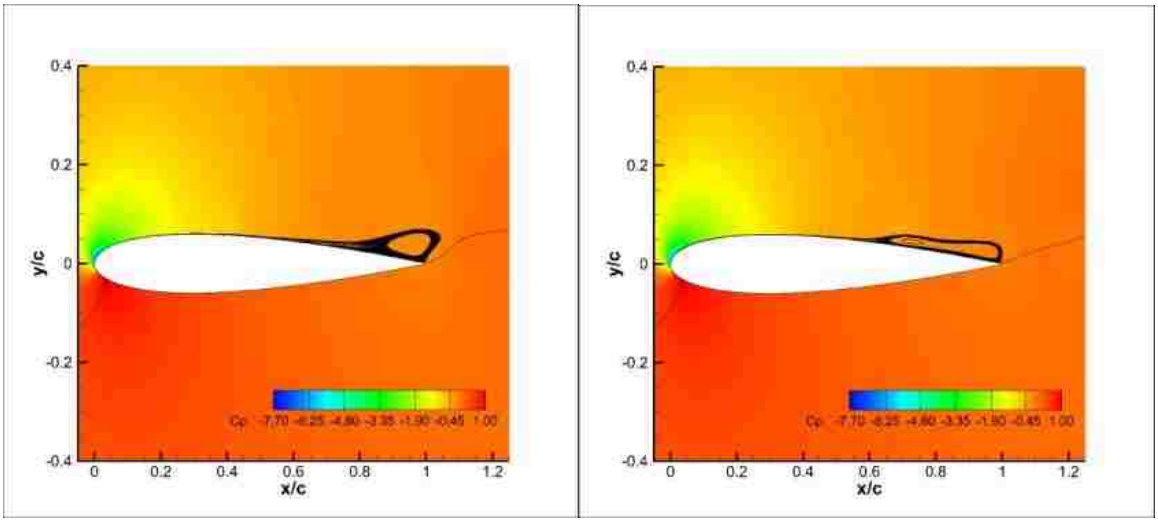

Figure 4.3: Pressure Coefficient Contours with Streamlines at 15 Degrees Angle of Attack with One Unsteady Actuator at 2% c. V = 15.13 kV kV, D = 50% (cont.)

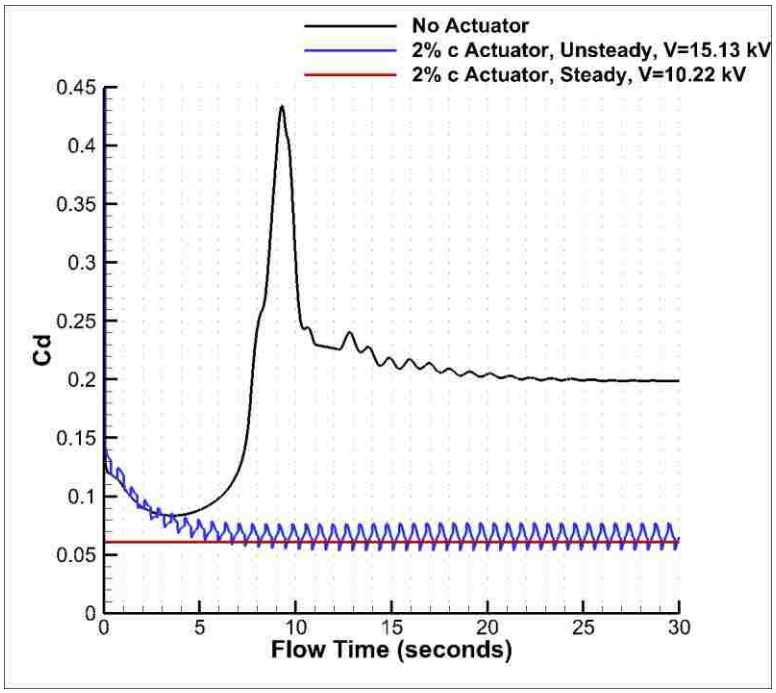

Figure 4.4: Drag Coefficient vs. Flow Time for a Single Unsteady Actuator at 15 Degrees Angle of Attack. V = 15.13 kV, D = 50%

4.3. INVESTIGATION OF FLOW CONTROL WITH MULTIPLE, STEADY ACTUATORS

The results for the cases with multiple, steady actuators are quite similar to the cases involving a single, steady actuator in terms of decreasing the size of the separation region. This is due to the fact the effect of multiple actuators is additive with regards to the total body force. Actuators with 10.22 kV input produce a force of about 16 mN/m. With two actuators, this implies that there is a total of 32 mN/m produced by the pair. This corresponds to an input voltage of 15.13 kV for a single actuator which was the highest voltage analyzed for a single actuator. Figure 4.5 gives the pressure contours with stream traces.

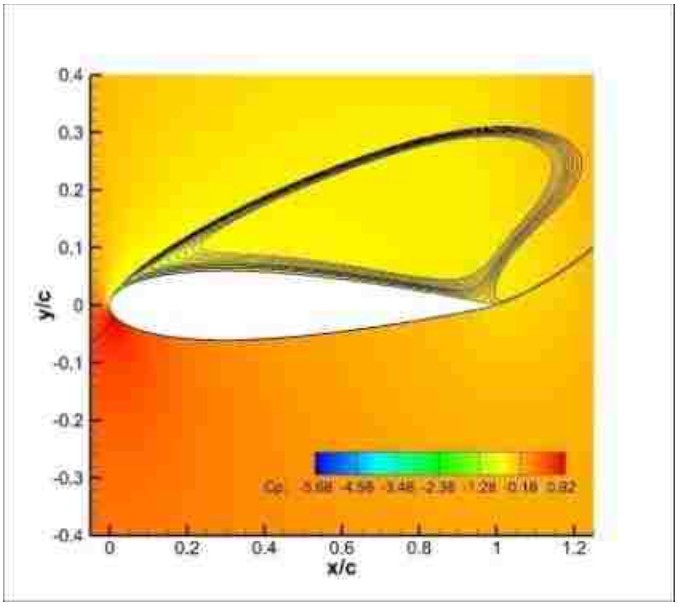

a) No Actuator

Figure 4.5: Pressure Coefficient Contours with Streamlines of Two Steady State Actuators at 10 Degrees Angle of Attack. V = 7.77 kV each, Left. V = 10.22 kV each, Right

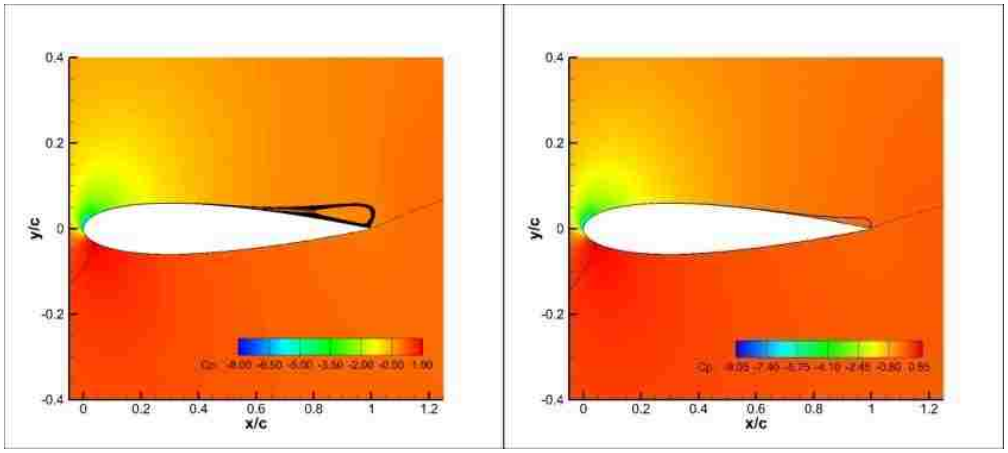

b) 2 and 4% Chord Actuators

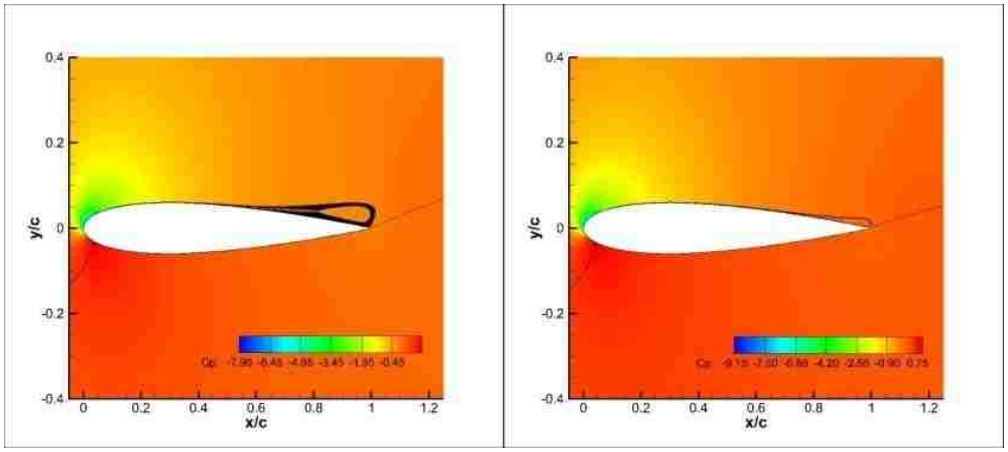

c) 2 and 6% Chord Actuators

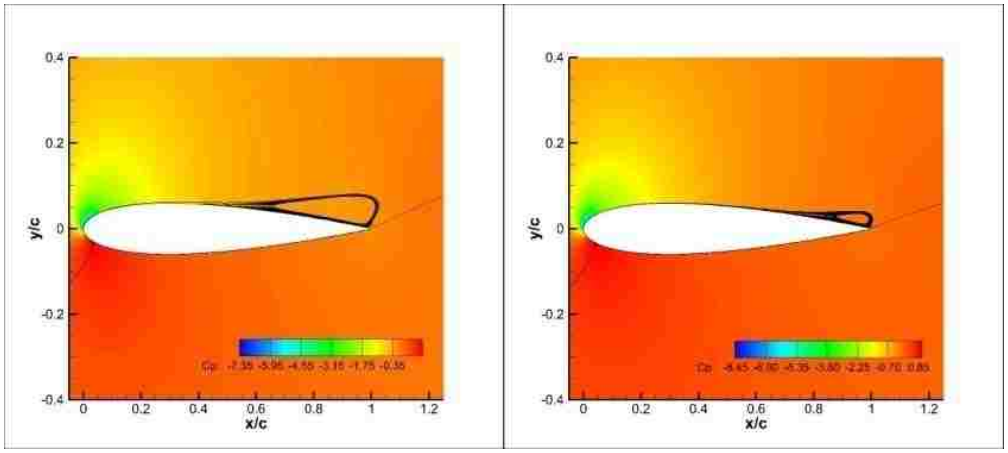

d) 4 and 6% Chord Actuators

Figure 4.5: Pressure Coefficient Contours with Streamlines of Two Steady State Actuators at 10 Degrees Angle of Attack. V = 7.77 kV each, Left. V = 10.22 kV each, Right (cont.)

The best cases (highest L/D) shown in the case with actuators at 2% and 4% of the chord each with a 10.22 kV input. Comparing this case to the single 2% chord actuator case a 15.13 kV input shows that there are some slight differences. The L/D ratio is about 16% higher for the single actuator case. With regards to the lift, the suction near the leading edge is not as substantial with the lower powered actuators and therefore the lift is not as high when compared to the single actuator case. However, there is only about a 3% difference in the lift. The big deficit comes from the drag. This is because the separation region reaches about 13% further upstream for the multiple actuator case. This increases the drag by nearly 11%.

4.4. INVESTIGATION OF FLOW CONTROL WITH MULTIPLE, UNSTEADY ACTUATORS

Similar observations made for the single unsteady actuator cases can also be made for the multiple unsteady actuator cases. The unsteady actuators do not provide significant improvement compared to steady actuators. The pulsing effect does not induce a vortex shedding process as a region of separation remains attached to the trailing edge. Like with the single, unsteady actuators, multiple, unsteady actuators are able to keep the separation confined to the trailing edge which does provide significant enhancement in aerodynamic performance (L/D), though the same improvement as single for steady actuator cases is not seen. L/D values for each to the analyzed configurations are given in Table 4.2. Figure 4.6 shows periodic behavior for a multiple actuator configuration compared to a single, steady actuator of the same time averaged body force.

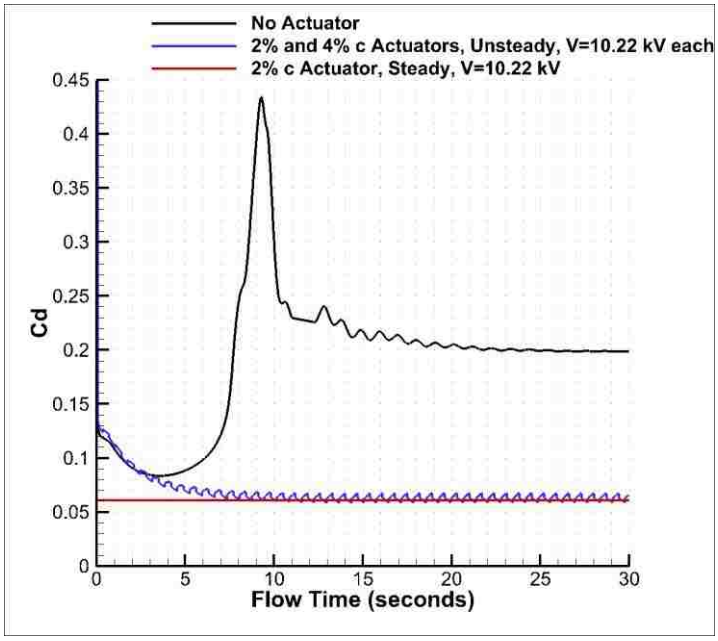

Figure 4.6: Drag Coefficient vs. Flow Time for Multiple, Unsteady Actuators at 15 Degrees Angle of Attack. V = 10.22 kV each, D = 50%

4.5. SUMMARY OF THE RESULTS

4.5.1. Plasma Actuator Location. Overall, similar trends are observed as with the laminar separation cases, most importantly with regards to actuator placement. Even though all of the actuator configurations are capable of providing significant improvement to the aerodynamic performance of the airfoil, the most efficient and effective approach is to ensure that the actuator is located upstream of any separation that may be present in the flow. The results in Table 4.1, as well as the figures throughout this chapter suggest that it is possible to the control separated flow coming from the trailing edge using leading edge actuators. As long as the added momentum from the plasma actuator is sufficient enough to keep the separation region from moving forward over the maximum thickness of the airfoil, then the significant loss in aerodynamic performance associated stall conditions (substantially decreased lift and increased drag.) This conclusion explains why a significant increase in L/D (Table 4.1) is observed of nearly every case investigated. Each configuration has the ability to suppress the separation region given a high enough voltage input.

4.5.2. Steady vs. Unsteady Plasma Actuators. In general, the steady state actuators outperform unsteady actuators both in terms of effectiveness and efficiency as even unsteady actuators with the same time averaged force magnitude as a single actuator cannot provide the same level of aerodynamic improvement. This is quite the opposite that was observed for the control of laminar separated flows, where the unsteady actuator was, in every case, more effective and efficient in improving the aerodynamic performance compared to a steady actuator at the same time averaged force magnitude. Also, note that the most improvement was achieved from using the actuator nearest to the leading edge. Not only does this provide the most improvement in the suction on the leading edge, but, after the trailing edge separation is forced downstream, a small region of separation stands near the leading edge which only the farthest forward actuator was the ability to prevent.

4.5.3. Effect of Multiple Plasma Actuators. Overall, there is not a substantial gain to using multiple actuator configurations for this particular case. For multiple, steady actuators the reduction in the separation region size is similar for a single, steady actuator with the same total, additive, body force. However, the improvement in the suction is not as substantial as the as half of the added momentum is further away from the leading edge. The same effects are seen for multiple, unsteady actuators compared to a single, unsteady actuator where the disturbances generated by the pulsing effect do suppress the separation region from covering the entire upper surface, however, the aerodynamic improvement is not as significant compared to a single, steady actuator at the same power consumption.

5. CONCLUSIONS AND FUTURE WORK

5.1. CONCLUSIONS

The primary objective of this study was to investigate and demonstrate the effectiveness of aerodynamic plasma actuators as a means of active flow control over airfoils over a range of angles of attack. This included analyzing two flow scenarios that are detrimental to aerodynamic performance: laminar separation bubbles at a low angle of attack and turbulent separation at stall conditions. Results were obtained for actuators operating in both steady and unsteady modes, as well as multiple actuator configurations.

For the laminar separation bubble cases, successful reduction in separation size was achieved resulting in as much as a 45% recovery of the lift to drag ratio, depending on the angle of attack. Results also indicate that with the use of a single, unsteady actuator the same, if not slightly more improvement can be achieved with as little as 25% of the body force magnitude of a single, steady actuator. In all cases, unsteady actuators provide as much as a 12% improvement over a single actuator at the same time averaged body force magnitude. This reduction in the body force magnitude is synonymous to a reduction in the power required to drive the plasma actuator. These results are comparable to the results found by Aholt [20] where as much as a 60% improvement in the lift to drag ratio was achieved over an elliptical airfoil. Aholt also observed that unsteady actuators provide as much as a 19% improvement over equivalently powered steady actuators. The improvement with the unsteady actuators is due to an induced, periodic vortex shedding process which prevents large scale separation from occurring. Similar trends are seen for the multiple actuator configurations (both steady and unsteady.) Nearly the same aerodynamic improvement is achieved for multiple actuator configurations as with steady actuator configurations at the time averaged body force magnitude, with the same mode of operation.

Another important conclusion drawn from these results was the dependence on actuator location relative to the separation region. It was found that if the actuator was located inside the separation region, it may not be effective at all. If separation control can be achieved, it comes at a great cost in terms of required power. The optimum location for an actuator would be just upstream of the separation location. This is where

the usefulness of multiple actuator systems becomes clear. In a dynamic environment, the separation location maybe changing, especially in laminar separated flows where the separation location propagates upstream with increasing angle of attack. In this case, a single actuator maybe not be able to control the flow separation across the range of angles of attack, both effectively and efficiently. Multiple actuator systems may also be useful in scenarios where a single actuator can only by prevent separation for a short distance downstream. An array of actuators would allow for continuous propagation of the separation location. This suggests that the use of multiple actuator configurations may be the most practical design for aerospace applications that operate in this flow regime.

For turbulent separated flow at stall conditions, similar trends were observed for single, steady actuators. For the cases studied, as much as a 700% improvement in L/D was achieved. This is primarily due to the suppression of the separation region towards the trailing edge as well as the increased suction on the leading edge. Multiple, steady actuators have a similar effect when compared to a single, steady actuator of same additive body force. While the reduction in the separation region size may be the same between the two, the L/D enhancement is not as great for multiple, steady actuators as the suction on the leading edge is not as substantial.

However, the same improvement could not be achieved with unsteady actuation, whether with a single actuator or multiple actuators. While there is significant improvement compared to the uncontrolled case, that improvement is not as much as is achieved from steady actuators. This is because of the nature of the separation region, which originates in the trailing edge region rather than the leading edge. The same periodic vortex shedding seen with the laminar separated flows is not observed in this case. The unsteady actuator creates a periodic swelling and deflating effect on the trailing edge separation, however never causing detachment. In a case where the separation was coming from the leading edge (at a lower Reynolds number or with a different geometry) and the separation location was only being pushed slightly downstream by a single actuator, multiple actuators may prove to be an effective alternative to continuously move the separation location downstream as far as required to maintain attached flow.

5.2. FUTURE WORK

The future work may include performing the analysis with a high-fidelity CFD model beyond RANS simulations such as Large-Eddy simulations (LES), RANS/LES hybrid methods, or even direct numerical simulations. The advantage of the ladder would be better quantification of the turbulent flow structure, as this is not really possible with simple RANS modeling. However, the effect of the plasma actuator should remain relatively the same.

A second potential work would be to use a more sophisticated and physically, more representative model for the plasma actuator. The plasma actuator can be represented using the Maxwell equations for electromagnetism. Developing a model that represents the physics of the plasma actuator using these equations could then be coupled to the equations that govern fluid flow, which would result in a much higher fidelity representation of the behavior and effects of plasma actuators.

Also, an import step would be to develop an experimental setup to determine the validity of, not only results found in this study, but any higher order simulations that are developed. The use of plasma actuators has already been performed in several previously discussed experiments. However a comparison with numerical analyses has not been widely done. An experimental analysis would help to determine if the simple model used in this study is sufficient enough or if a higher order model is necessary to better represent the effects of plasma actuators.

The potential uses and configurations of plasma actuators are diverse. Much analysis needs to go into determine the geometric effects on the effectiveness of plasma actuators, especially with regards to airfoil shape. In this study many different actuator configurations were examined, but there may be other possibilities. For example, future work may investigate the use a mixture of steady and unsteady actuators, or actuators on both the leading and the trailing edge. It is hoped that this study will provide a great foundation for future work, which may further investigate and characterize the capabilities and applications of plasma actuators for aerodynamic flow control.

APPENDIX A.
CFD SETUP PROCEDURE

The purpose of this appendix is to give a step by step procedure for setting up the cases in ANSYS FLUENT 12 used in this study. Snapshots of each step are given to aide in the explanation of each step.

Step 1: Read in the computational grid (File > Mesh).

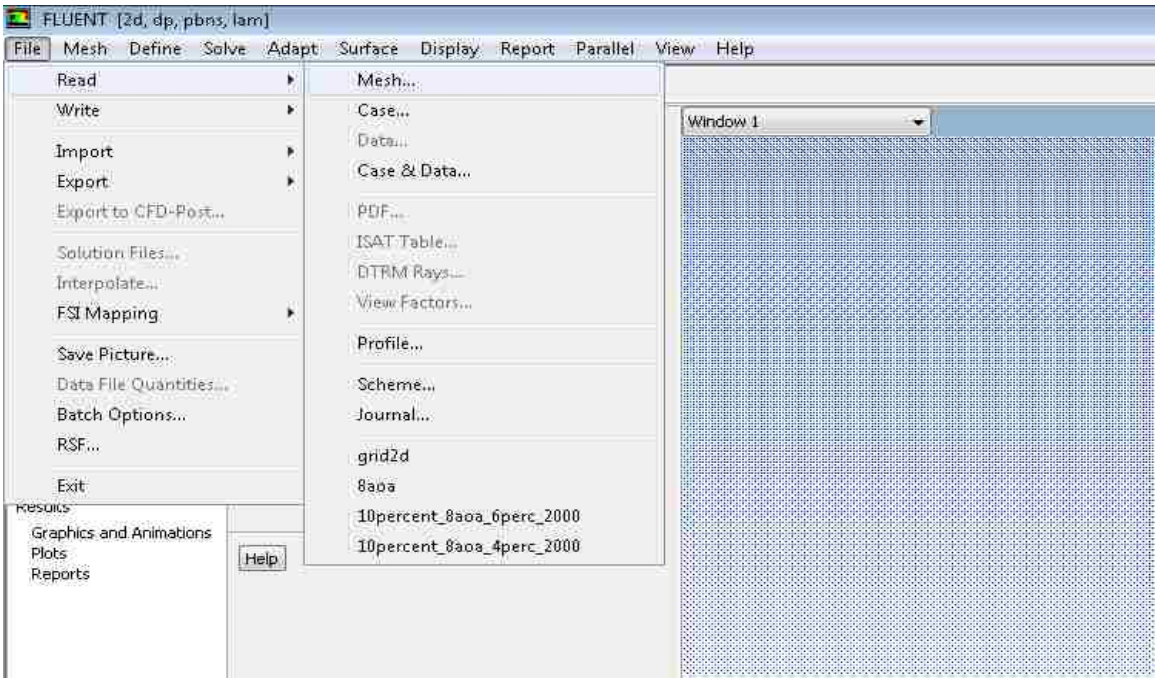

Step 2: Check Mesh. Select Pressure-Bases solver and the solver time. If the case is for unsteady actuation, select "Transient."

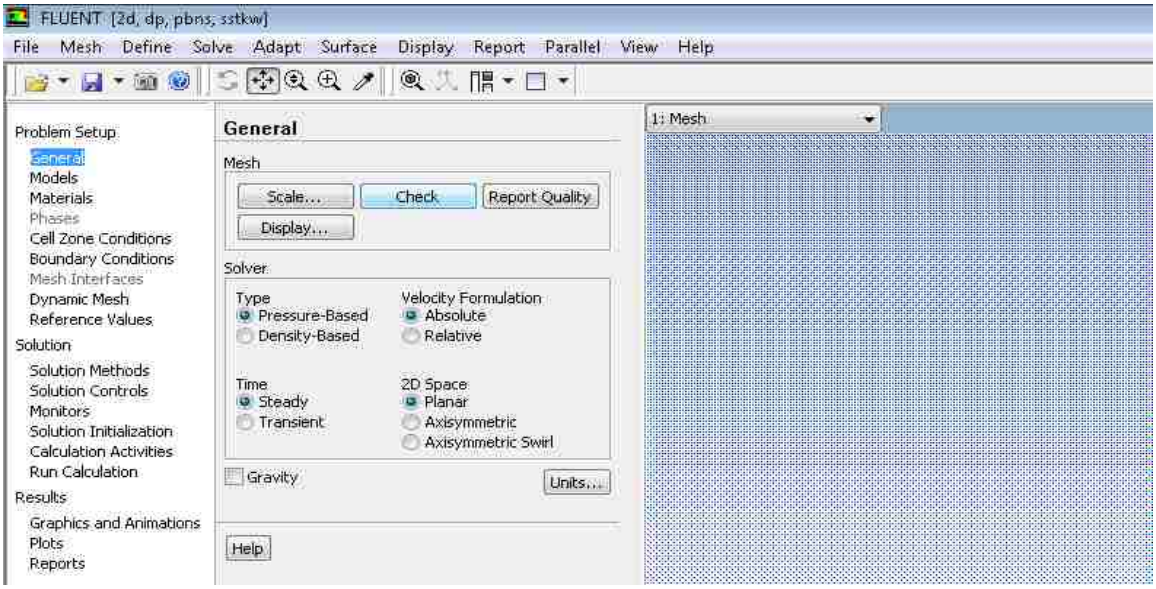

Step 3: Under Models select Viscous and choose the Spalart-Allmaras (1 eqn) model. The default setting were sufficient for this study.

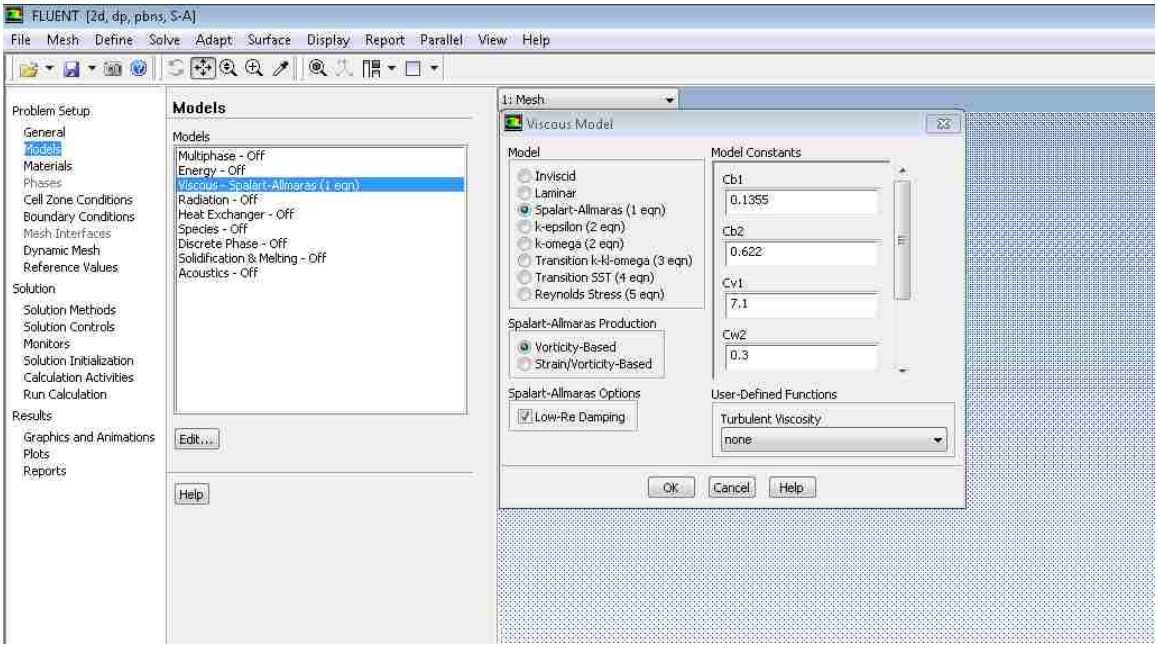

Step 4: (Optional for Laminar-Turbulent boundary imposition). Under Cell Zone Conditions select the upstream zone (previously partitioned in grid generation software) and then select laminar zone.

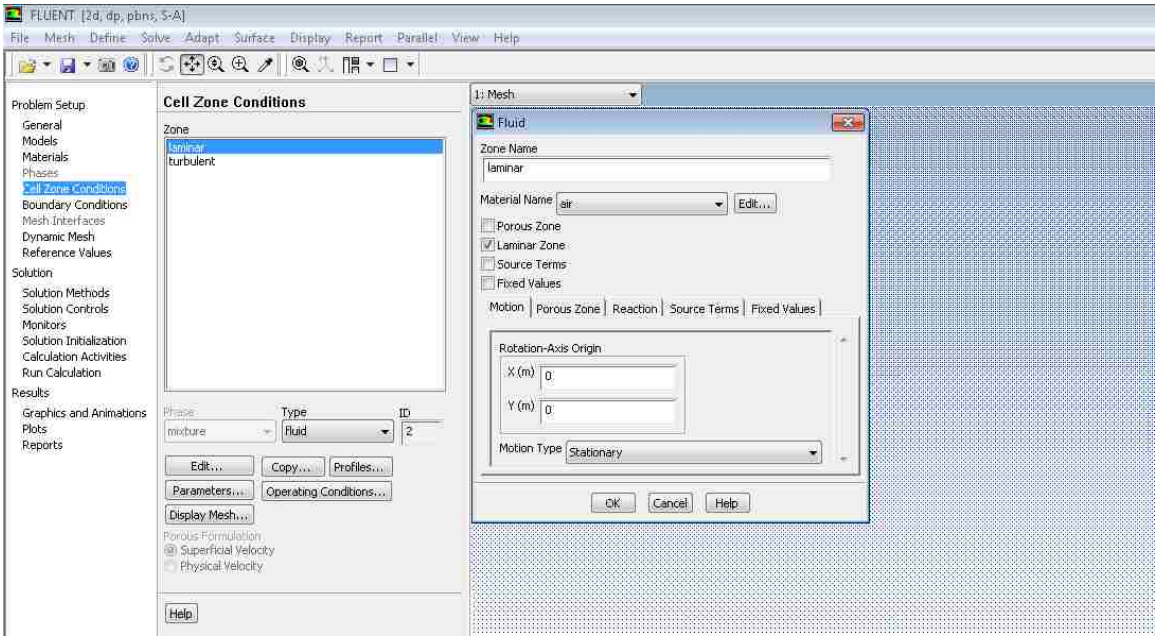

Step 5: Under Boundary Conditions select the inlet boundary and set the free-stream velocity and Turbulence level. Note that the default air properties are sea level quantities. Also set the reference values from the inlet.

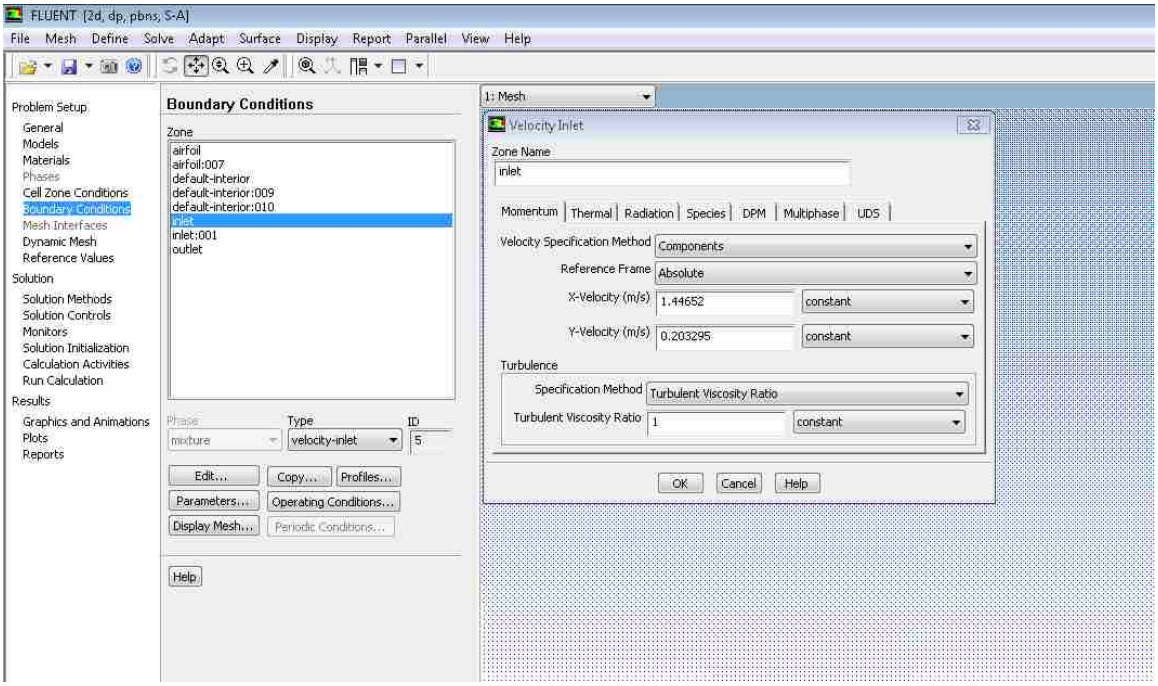

Step 6: Set the Spatial Discretization for of the governing equations. Also set the Pressure-Velocity Coupling to SIMPLE.

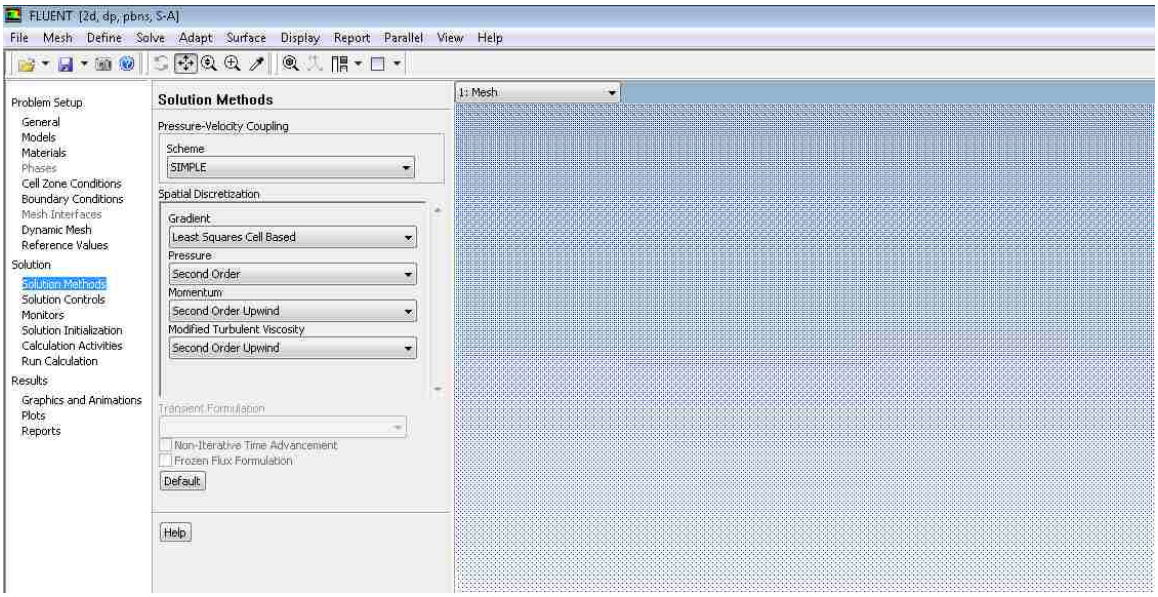

Step 7: Under Monitors, set the convergence requirement for the residuals.

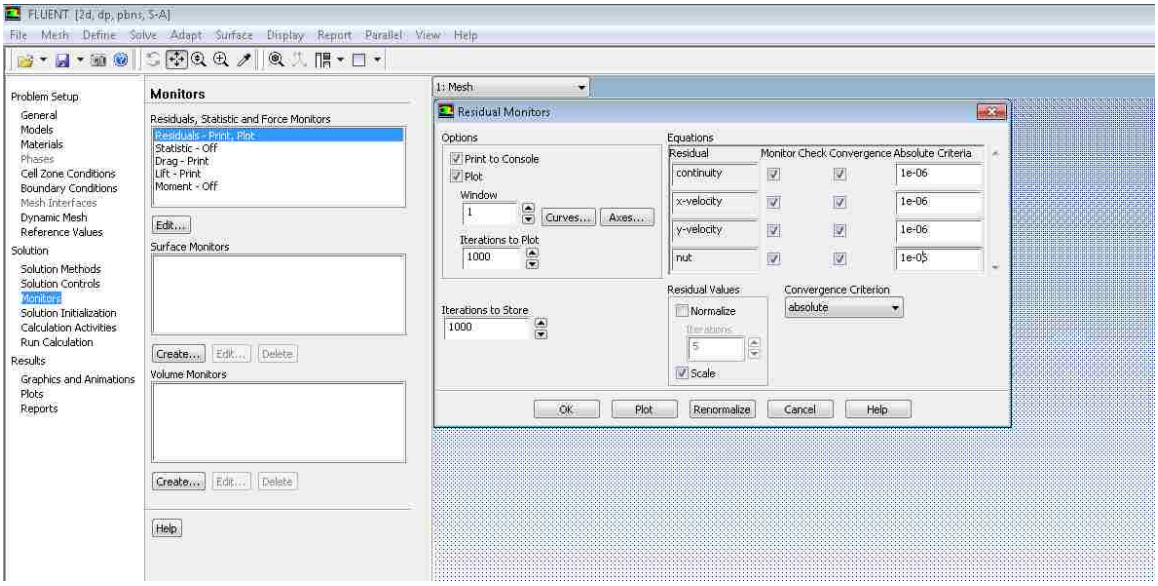

Step 8: Compile the UDF (Define > User-Defined > Functions > Complied). Add the source file and select build. After successful compilation select load.

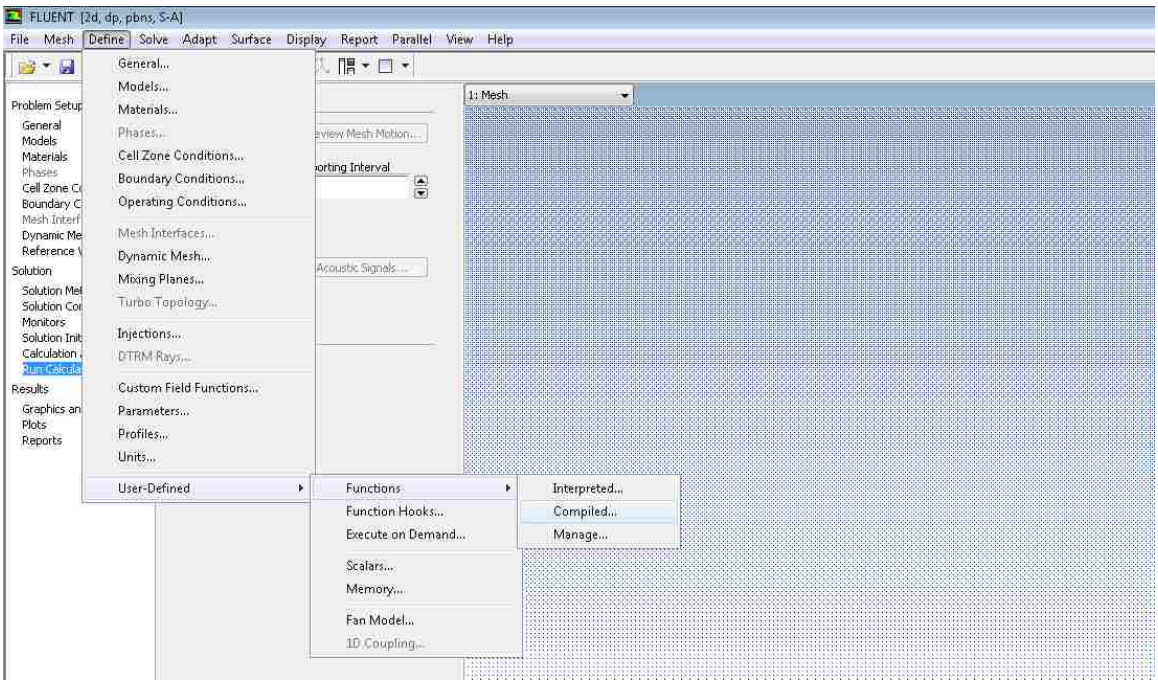

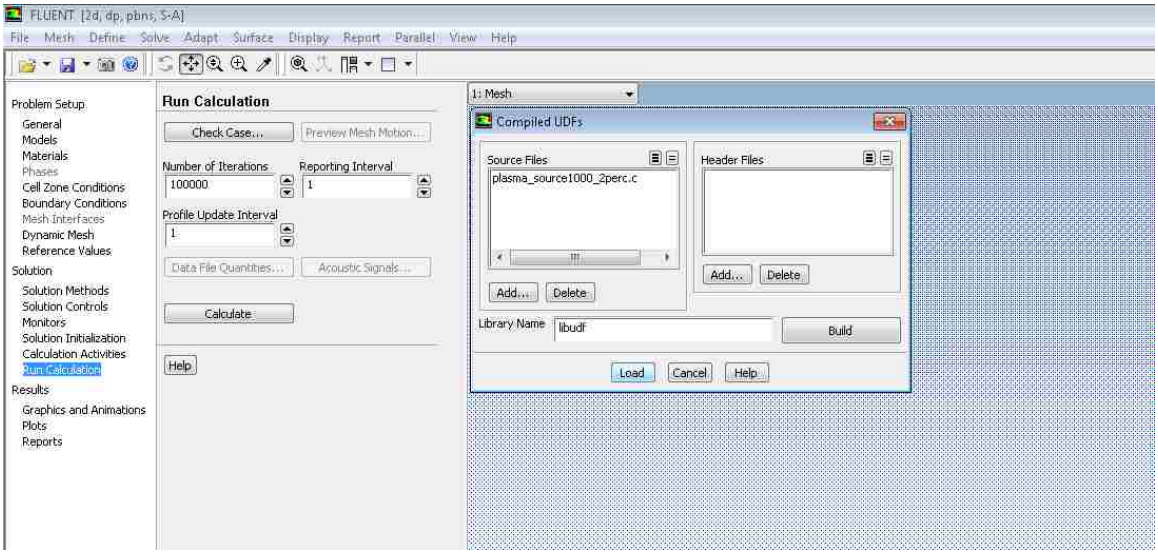

Step 9: Link the UDF. Under Cell Zone, select the zone where the source is located. Check Source, and then under the source tab selected the compiled UDF.

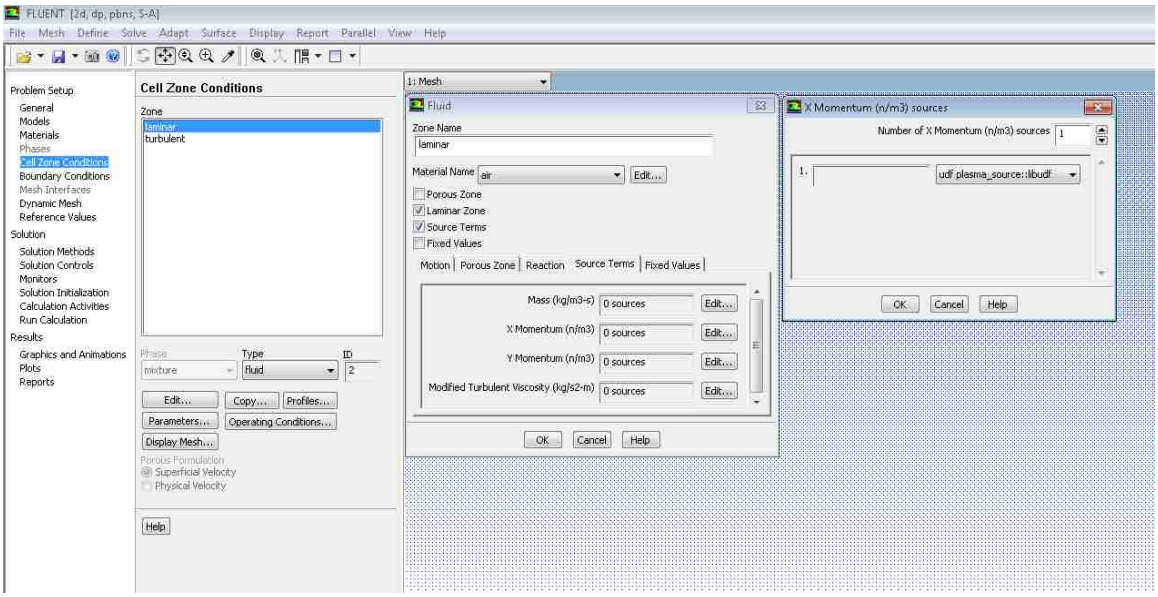

Step 10: Initialize the solution from the inlet. Then under Run Calculation set the number of iterations and select solve. Note for unsteady cases the time step size, number of time steps and number of iterations per time step must be set.

APPENDIX B.
PLASMA ACTUATOR UDF

The purpose of this appendix it to give an example of the UDF used to incorporate the momentum source term that represents the body force produced by the plasma actuator. UDF are written in C and compiled by FLUENT. This example is for a 2% chord steady actuator. For unsteady actuators the only difference is that the activation of the source term is restricted by the flow time. Extra IF statements (IF flow_time > some_time) around the source term allow for time dependent actuation.

```
#include "udf.h"
DEFINE_SOURCE(plasma_source,c,t,dS,eqn)
{
/* Declare Variables */
  real xc[ND_ND];
  real source, x, y;
  real m1, m2;
  real b_bottom, b_left, b_top, b_right;
  real check_bottom, check_left, check_top, check_right;
/* Call x and y data from FLUENT */
  C_CENTROID(xc,c,t);
  x=xc[0];
  y=xc[1];
/* Define plasma region. Four inequalities are used to define the rectangular plasma region. */
  m1=0.4859;
  m2=-2.0581;
  b_bottom=0.0139;
  b_left=0.0648;
  b_top=0.0140;
  b_right=0.0876;
  check_bottom=m1*x+b_bottom;
  check_left=m2*x+b_left;
  check_top=m1*x+b_top;
```

```
  check_right=m2*x+b_right;
/* Apply source term to region inside the four inequalities */
  if ((y>=check_bottom)&&(y>=check_left)&&(y<=check_top)&&(y<=check_right))
  {
    source = 1000.0;
    dS[eqn] = 0;
  }
  else
  {
    source = 0;
    dS[eqn] = 0;
  }
  C_UDMI(c,t,0)=source;
  return source;
}
```

BIBLIOGRAPHY

[1] Suzen, Y. B., Huang, P. G., and Jacob, J. D., "Numerical Simulations of Plasma Based Flow Control Applications," AIAA-Paper 2005-4630, *35th AIAA Fluid Dynamics Conference and Exhibit*, Toronto, Ontario Canada.

[2] Corke, T. C., Post, M. L., and Orlov, D. M., "SDBD plasma enhanced aerodynamics: concepts, optimization and applications," *Computers & Fluid*, Vol. 43, 2007, pp. 193-217.

[3] Corke, T. C., and Post, M. L., "Overview of Plasma Flow control: Concepts, Optimization and Applications," AIAA-Paper 2005-563, *43th AIAA Aerospace Sciences Meeting and Exhibit*, Reno, Nevada.

[4] He, C., Corke, T. C., and Patel, M. P., "Plasma Flaps and Slats: An Application of Weakly Ionized Plasma Actuators," *Journal of Aircraft*, Vol. 46, No. 3, 2009, pp. 864-873.

[5] Enloe, C. L., McLaughlin, T. E., VanDyken, R. D., Kachner, K. D., Jumper, E. J., Corke, T. C., Post, M., and Haddad O., "Mechanisms and Responses of a Single Dielectric Barrier Plasma Actuator: Geometric Effects," *AIAA Journal*, Vol. 42, No. 3, 2004, pp.595-604.

[6] Shan, H., Jiang, L., Liu, C., Love, M., and Maines, B., "Numerical Study of Passive and Active Flow Separation Control Over a NACA 0012 Airfoil," *Computers & Fluid*, Vol. 37, 2008, pp. 975-992.

[7] Mabe, J. J., Calkins, F. T., Wesley, B., Taubert, L., and Wygnanski, I., "Single Dielectric Barrier Discharge Plasma Actuators for Improved Airfoil Performance," *Journal of Aircraft*, Vol. 46, No. 3, 2009, pp. 847-855.

[8] Aholt, J., and Finaish F., "Active Flow Control Strategy of Laminar Separation Bubbles Developed over Subsonic Airfoils at Low Reynolds Numbers," AIAA-Paper 2011-733, *49th AIAA Aerospace Sciences Meeting including the New Horizons Forum and Aerospace Exposition*, Orlando, Florida.

[9] Visbal, M. R., Gaitonde, D. V., and Roy, S., "Control of Transitional and Turbulent Flows Using Plasma-Based Actuators," AIAA-Paper 2006-3230, *AIAA Fluid Dynamics and Flow Control Conference*, San Francisco, California.

[10] Tsubakino, D., Tanaka, Y., and Fujii, K., "Effective Layout of Plasma Actuators for a Flow Separation Control on a Wing," AIAA-Paper 2007-474, *45th AIAA Aerospace Sciences Meeting and Exhibit*, Reno, Nevada.

[11] Huang, J., Corke, T. C., and Thomas, F. O., "Unsteady Plasma Actuators for Separation Control of Low-Pressure Turbine Blades," *AIAA Journal,* Vol. 44, No. 7, 2006, pp. 1477-1487.

[12] Benard, N., Bonnet, J. P., Touchard, G., and Moreau, E., "Flow Control by Dielectric Barrier Discharge Actuators – Jet Mixing Enhancement," AIAA 2008-3878, *4th AIAA Flow Control Conference,* Seattle, Washington.

[13] Thomas, F. O., Alexey, K., and Corke T. C., "Plasma Actuators for Landing Gear Noise Reduction," AIAA 2005-3010, *26th AIAA Aeroacoustics Conference,* Monterey, California.

[14] Porter, C. O., Baughn, J. W., McLaughlin, T. E., Enloe, C. L., and Font, G. I., "Temporal Force Measurements on an Aerodynamic Plasma Actuator," AIAA-Paper 2006-104, *44th AIAA Aerospace Sciences Meeting and Exhibit,* Reno, Nevada.

[15] Shan, H., Jiang, L., and Liu, C., "Direct Numerical Simulation of flow separation around a NACA 0012 airfoil," *Computers & Fluid,* Vol. 34, 2005, pp. 1096-1114.

[16] *ANSYS FLUENT User Manual.*

[17] Barth, T. J., Pulliam, T. H., and Buning, P. G., "Navier-Stokes Computation for Exotic Airfoils," AIAA-Paper 1985-109, *23rd AIAA Aerospace Sciences Meeting,* Reno, Nevada.

[18] Spalart, P. R., and Allmaras, S. R., "One-Equation Eddy-Viscosity Turbulence Models for Engineering Applications," AIAA-Paper 92-0439, *30th Aerospace Sciences Meeting and Exhibit,* Reno, Nevada.

[19] Nichols, T. G., and Rovey, J. L., "Fundamental Process of DBD Plasma Actuators Operating at High Altitude," AIAA-Paper 2012-0822, *50th AIAA Aerospace Sciences Meeting including the New Horizons Forum and Aerospace Exposition,* Nashville, Tennessee.

[20] Aholt, J. R., "Computational Investigation of Plasma Actuator as an Active Flow Control Strategy of Laminar Separation Bubbles." Master's Thesis, Missouri University of Science and Technology, 2011.

VITA

Thomas Kelsey West IV was born in Lake St. Louis Missouri. After graduating from Troy Buchanan High School in Troy, MO in 2006, he began his undergraduate education at the Missouri University of Science and Technology. Over the course of his undergraduate education, he was selected for the NASA Undergraduate Student Research Program where he spent a semester at NASA's Jet Propulsion Laboratory in 2008. In 2010, Thomas graduated Summa Cum Laude earning Bachelor of Science degrees in both Aerospace Engineering and Mechanical Engineering as well as an undergraduate minor in Applied Mathematics. He then continued his education earning a Master of Science degree in Aerospace Engineering from the Missouri University of Science and Technology in 2012.